Journal of Hydrology 641 (2024) 131772

Contents lists available at ScienceDirect

Journal of Hydrology

journal homepage: www.elsevier.com/locate/jhydrol

Research papers

Hydrologic sustainability of a mediterranean tree-grass ecosystem under climate change

Nicola Montaldo *, Roberto Corona

Dipartimento di Ingegneria civile, ambientale e architettura, Università di Cagliari, Italy

ARTICLE INFO

This manuscript was handled by Corrado Corradini, Editor-in-Chief, with the assistance of Xuan Yu, Associate Editor

Keywords:
Climate change
Ecohydrologic model
Wild olive
Tree-grass ecosystem
Leaf area index
Evapotranspiration

ABSTRACT

In Mediterranean dryland ecosystems climate change is occurring with an increase in air temperature and a decrease (mainly in wet seasons) of precipitation, which are key for grass and tree growth. We investigated an attractive Sardinian case study with a typical tree-grass ecosystem, where wild olives and seasonal grass species grow on thin surface soil layer overlaying a fractured rock sublayer. A very long-term database with almost 60 years of data is available, with micrometeorological and meteorological measurements, and remote sensing data, providing a unique opportunity to analyze the response of tree-grass ecosystems to historical climate and land cover changes. We proposed an ecohydrological model that was able to reproduce the soil, vegetation, and atmosphere interactions and dynamics, and their long-term evolution. The model accurately predicted the long-term dynamics of the tree cover fraction, which was drastically reduced (~0.10) by a human-induced fire about 50 years ago, and restored naturally in almost 20 years, reaching the equilibrium value (~0.33). The Sardinian tree-grass ecosystem suffered a historically significant reduction in rain and a significant increase in air temperature in the last century. The predicted future scenarios are even more severe, with a further decrease of mean annual precipitation (MAP) of up to ~400 mm, and an increase of air temperature of +4 °C, which will cause a reduction of the tree cover fraction of up to 0.10 and a strong decrease of the tree LAI. At present, the developed tree cover percentage of the Sardinian site is sustainable with the historical MAP (>600 mm/y), thanks to the tree hydraulic redistribution contribution to transpiration (up to 80 %). In the predicted future scenarios, the increase of dry conditions with a wetness index (precipitation/potential evaporation) below 0.005 will increase the hydraulic redistribution contribution, reaching 91 % of tree transpiration, which, however, will be not enough to support tree growth and maintenance. The soil is predicted to become drier, with less grass and vegetation in general, with consequences for the landscape aspect, becoming more and more a savanna-like ecosystem.

1. Introduction

Dryland ecosystems are widely spread all around the world (~47 %, D'Odorico et al., 2019). These ecosystems are highly sensitive to seasonal and decadal climate changes, which can impact water availability (D'Odorico et al., 2019) and ecosystem sustainability (Yaseef et al., 2010; Grossiord et al., 2017; Montaldo et al., 2021). In Mediterranean basin ecosystems, climate change is manifesting itself mainly with a positive trend of air temperature, and a negative trend of precipitation in wet seasons (Martínez-Fernández et al., 2013; Montaldo and Sarigu, 2017; Corona et al., 2018). Climate predictions of future scenarios by the Intergovernmental Panel on Climate Change (IPCC) are more dire, affecting the central Mediterranean basin with a further decrease of rainfall in wet months and an increase in air temperature (Ozturk et al., 2015; Lionello and Scarascia, 2018; Sirigu and Montaldo, 2022). Mediterranean regions are highly sensitive to climate change (Giorgi and Lionello, 2008), and were classified by Giorgi (2006) as one the most pronounced "hot spots" in the world, being affected by changes of both precipitation and evaporation (highly related to air temperature), the two asynchronous atmospheric forcing impacting the soil water balance (Montaldo and Oren, 2018).

Mediterranean regions are water-limited ecosystems characterized by the coexistence of trees and grasses that compete for water use, and their spatial distributions are affected by physiographic properties and atmospheric forcing, and evolve in time with climate dynamics (Scholes and Archer, 1997; Kurc and Small, 2004; Sankaran et al., 2005;

* Corresponding author at: Dipartimento di Ingegneria civile, ambientale e architettura, Università di Cagliari, Via Marengo, 3, I-09123 Cagliari, Italy.
E-mail address: nmontaldo@unica.it (N. Montaldo).

https://doi.org/10.1016/j.jhydrol.2024.131772
Received 8 March 2024; Received in revised form 4 July 2024; Accepted 21 July 2024
Available online 6 August 2024

Breshears, 2006; Detto et al., 2006; Montaldo et al., 2008; Moore and Heilman, 2011; Villegas et al., 2014). Indeed, in these ecosystems climate seasonality plays a central role, controlling the hydrological sustainability of trees, with wet seasons providing water needs for sustaining vegetation growth and its subsistence during dry seasons. Climate change is impacting the seasonality of the climate, both rain and air temperature, and these changes may impact the delicate equilibrium of tree-grass ecosystems (Scholes and Archer, 1997; Sankaran et al., 2005; Breshears, 2006; Detto et al., 2006; Montaldo et al., 2008). In these ecosystems, during wet seasons rain infiltrates into deep soil layers, providing a water supply for tree livelihood in dry seasons when tree roots uptake water from the underlying soils through the hydraulic lift phenomenon (Domec et al., 2010; David et al., 2013; Nadezhdina et al., 2015; Sperry and Love, 2015; Fan et al., 2017; Montaldo et al., 2021). In those ecosystems trees often grow on thin soils above fractured rocks, with tree roots penetrating into the sublayer of fractured rocks for water uptake. Indeed, in these conditions, evapotranspiration is mainly supplied (up to 70–90 %) by rock water storage (Schwinning, 2010; Yu and D'Odorico, 2014; Nie et al., 2017; Eliades et al., 2018; Rempe and Dietrich, 2018; Montaldo et al., 2021). Hence, changes of annual and seasonal climate may impact the perspective of tree sustainability and the delicate hydrological equilibrium that supports vegetation growth in dryland ecosystems (Scholes and Archer, 1997; Sankaran et al., 2005; Breshears, 2006; Detto et al., 2006; Montaldo et al., 2008). The estimated declining trend of rain in many Mediterranean regions (Martínez-Fernández et al., 2013; Montaldo and Sarigu, 2017) can affect tree sustainability (Doughty et al., 2015; Clark et al., 2016). Sankaran et al. (2005) and Axelsson and Hanan (2017) estimated a mean annual precipitation (MAP) threshold of around 600–700 mm, below which rain restricted tree cover growth in African savannas. At the same time, an increase of vapor pressure deficit (VPD) due to the recognized increase of air temperature may affect vegetation growth negatively (Williams et al., 2013; Yuan et al., 2019). Future climate change scenarios are predicting drier conditions (Ozturk et al., 2015; Lionello and Scarascia, 2018; Sirigu and Montaldo, 2022) that can affect tree development, making past survival and water-use optimization strategies insufficient, and these need to be investigated carefully.

Long-term hydrological databases are important for understanding and evaluating past climate changes, and can be also the basis for properly modeling land surface fluxes under future climate scenarios. Nowadays, long-term databases of past land surface fluxes and remote sensing observations are starting to be available. Several experimental sites have been instrumented from the early 2000s by eddy covariance towers for monitoring evapotranspiration, energy balance, soil water, and CO_2 exchanges (Baldocchi, 2003, Detto et al., 2006), and data for more than 20 years are available today (Baldocchi et al., 2021; Pang et al., 2021; Yang and Lei, 2022; Zheng et al., 2023). Some optical remote sensors, like Landsat (spatial resolution of 15–30 m) and the NOAA advanced very high-resolution radiometer (AVHRR) (spatial resolution of 1100 m), have been operating since the early 1980s (Gim et al. 2020; Ngadze et al. 2020), becoming useful for detecting vegetation cover changes. In dryland ecosystems, to capture the spatial variability of the typical tree-grass mosaic of the landscape, remote optical sensing data need to be at fine spatial resolutions (Hill et al., 2011; Olsoy et al., 2017), which can be achieved through the use of Landsat data, for example (Li et al., 2017; Ngadze et al., 2020), characterized by a temporal resolution of 16 days, which is enough to monitor seasonal vegetation dynamics (Montaldo et al., 2023). At the same time, historical aerial photographs are available in many areas of the world, mainly from the second world war, which do not with the same high frequency but are still relevant for capturing the long-term evolution of the land cover (Gennaretti et al., 2011; Mboga et al., 2020; Giza et al., 2021; Sirigu and Montaldo 2022). Merging these databases, climate change effects on vegetation cover dynamics in the past can be investigated (Barbeta et al., 2013; Clark et al., 2016; Sirigu and Montaldo, 2022). At the same time, investigating and estimating past land cover changes, and understanding of the climate causes of eventual natural historical land cover changes, can be a useful tool for properly predicting future changes and impacts on land surface fluxes and landscape ecosystems. In this sense, robust ecohydrological models opportunely tested using such long-term hydrological databases can be an important means for predicting the impacts of climate change.

Ecohydrological models have been developed in the last decades to account vegetation dynamics and their interactions with soil and atmosphere in land surface models. Ecohydrological models couple land surface models (LSM) and vegetation dynamic models (VDM) so that vegetation variables (e.g., the leaf area index, LAI) are simulated dynamically by the VDM and used by the LSM for hydrological process predictions (e.g., evapotranspiration, interception) (Cayrol et al., 2000; Nouvellon et al., 2000; Arora, 2003; Montaldo et al., 2005; Montaldo et al., 2008). Recently, Montaldo and Oren (2022) developed an ecohydrological model that is very useful in water-limited tree-grass ecosystem because it also predicts water uptake by tree roots from the fractured rock sublayer and, in general, from any deeper soil medium, and the hydraulic redistribution (HR) between the sublayer and surface soil, accounting for the heterogeneity in surface soil moisture caused by the rhizosphere. Montaldo and Oren (2022) demonstrated the importance of using a detailed ecohydrological model that includes HR and rhizosphere water balance to predict evapotranspiration and tree and grass behavior in a tree-grass Mediterranean ecosystem in Sardinia. For long-term predictions, because vegetation cover may change due to climate factors and vegetation species compete for light and natural resources (e.g., water) (Sitch et al. 2003), ecohydrological models need to include representation of the processes at the base of the evolution of vegetation cover. Global vegetation models include the dynamics of population density and vegetation cover at coarse spatial resolutions (Sitch et al., 2003; Gerten et al., 2004; Reick et al., 2013; Zhu et al., 2015), using accurate mathematical representation of the involved physical processes, which may overparameterize and increase the model computational burden for hydrologic applications. There is still a need for ecohydrological models characterized by simplicity and low parameterization that are still able to capture the main ecohydrological processes for long-term predictions. Furthermore, only the use of long-term database at a fine spatial scale can guarantee proper validation of ecohydrological models that suffer from over-parametrization.

Sardinia is an interesting case study of climate change impacts due to its position in the center of the Mediterranean Sea, its high sensitivity to climate change (Piras et al., 2014; Montaldo and Sarigu, 2017; Montaldo and Oren, 2018; Marras et al., 2021), its relatively low urbanization and human activity (with ~50 % of the total area covered by forest; Salis et al., 2015), and the lack of relevant land cover changes (Sirigu and Montaldo, 2022). The alteration of land cover due to human activity was mainly by fires, which is a typical concern in the Mediterranean area (Fernandes, 2013; Verkaik et al., 2013).

A typical Mediterranean ecosystem in Sardinia (Detto et al., 2006; Montaldo et al., 2008; Montaldo et al., 2013; Montaldo et al., 2020), where wild olives and seasonal grass species grow on a thin surface soil layer overlaying a fractured rock sublayer, was investigated. A long-term database of micrometeorological, tree transpiration, and soil water content measurements is available (Montaldo et al. 2021). Our objectives were: 1) detect trends and changes in the past climate, and their eventual relationships with the evolution of tree cover spatial distribution for the typical tree-grass ecosystem; 2) develop and test an ecohydrological model for long-term predictions able to capture the evolution of tree cover spatial distribution; and 3) investigate the impact of past and future climate scenarios on soil water balance and tree hydrological sustainability of the Mediterranean ecosystem.

Wild olive is a common Mediterranean species (Lumaret and Ouazzani, 2001; Terral et al., 2004), and like other common Mediterranean tree species, developed an adaption strategy to droughts. Despite their strong resistance to droughts, we investigated the wild olive resilience to future climate scenarios and its hydrologic sustainability in the

Mediterranean environment.

2. Methods

2.1. The ecohydrological model

The ecohydrological model of Montaldo et al. (2008) and Montaldo and Oren (2022) is based principally on coupling a land surface model, which predicts the soil water balance and the energy balance among the soil, vegetation, and atmosphere, and a vegetation dynamic model (Cayrol et al., 2000; Nouvellon et al., 2000; Montaldo et al., 2005; Fig. 1). The model distinguishes three land cover components: tree, grass, and bare soil. The purpose of model coupling is to obtain grass and tree leaf area index (*LAI*) dynamics at daily resolution from the VDM to use as input, based on which the LSM computes energy and water partitioning between soil and vegetation on a half-hourly time scale. Details of the existing model are in Montaldo et al. (2005, 2008), Montaldo et al. (2013) and Montaldo and Oren (2022). We updated the VDM for predicting the long-term evolution of the fraction of tree cover. Model meteorological inputs are precipitation, air temperature, wind velocity, incoming shortwave radiation, air relative humidity, and photosynthetically active radiation (Fig. 1), and the parameters are defined in Table 1.

2.1.1. The land surface model

The soil water balance includes a surface soil layer [predicted using the force-restore approach of Noilhan and Planton (1989), as revised by Montaldo and Albertson (2001)], a first root zone soil layer, and a fractured rock sublayer extending to the depth of sinker tree roots (Montaldo and Oren, 2022). The root zone supplies the bare soil and vegetation with soil moisture for evapotranspiration and controls the infiltration and runoff mechanisms, through:

$$\frac{d\theta_{sl}}{dt} = \frac{1}{d_{sl}}\left[I - f_{bs}E_{bs} - f_t\xi_t E_{t,rh} - f_{v,g}\xi_{g,rh}E_{g,rh} - f_{v,g}(1 - \xi_{g,rh})E_{g,nrh} - E_w - D_r - HR\right], \quad (1)$$

where θ_{sl} is soil moisture of the surface layer, d_{sl} is the depth of the surface root zone soil layer, I is infiltration rate, D_r is the rate of drainage out of the bottom of the surface root zone, HR is hydraulic redistribution, represented as a vertical flux through tree roots between the underlying substrate and the surface soil layer (positive when downward), E_{bs} is bare soil evaporation, $E_{t,rh}$ is tree transpiration from the surface layer, partially controlled by the moisture in the rhizosphere volume of the surface soil layer (θ_{rh}), $E_{t,fr}$ is tree transpiration from the fractured rock layer, $E_{g,rh}$ and $E_{g,nrh}$ are the rates of grass transpiration with roots partitioned between the rhizosphere of tree root and the rest of the surface soil layer, respectively, through $\xi_{g,rh}$, the fraction of grass root water uptake from the rhizosphere volume of tree roots, E_w is wet canopy evaporation, f_t is the fraction of tree cover, $f_{v,g}$ is the fraction of grass cover, and f_{bs} ($=1 - f_t - f_{v,g}$) is the fraction of bare soil. The soil moisture of the underlying fractured rock layer (θ_{fr}) is predicted by:

$$\frac{d\theta_{fr}}{dt} = \frac{1}{d_{fr}}\left[D_r - f_t(1 - \xi_t)E_{t,fr} + HR - L_e\right], \quad (2)$$

where d_{fr} is the depth of the underlying fractured rock layer, L_e is the leakage below the tips of sinker roots in the rock sublayer, and ξ_t is the fraction of tree root water uptake from the surface soil layer. The θ_{rh} is predicted from the soil water balance of the rhizosphere:

$$\frac{d\theta_{rh}}{dt} = \frac{1}{d_{sl}}(I - D_r) - \frac{1}{d_{rh}}\left(f_t\xi_t E_{t,rh} + f_{v,g}\xi_{g,rh}E_{g,rh} + HR\right) \quad (3)$$

where d_{rh} is the depth of the rhizospheres in the d_{sl} soil depth.

Both D_r and L_e are estimated using the unit head gradient assumption (Albertson and Kiely, 2001), so that a gravitational drainage is predicted

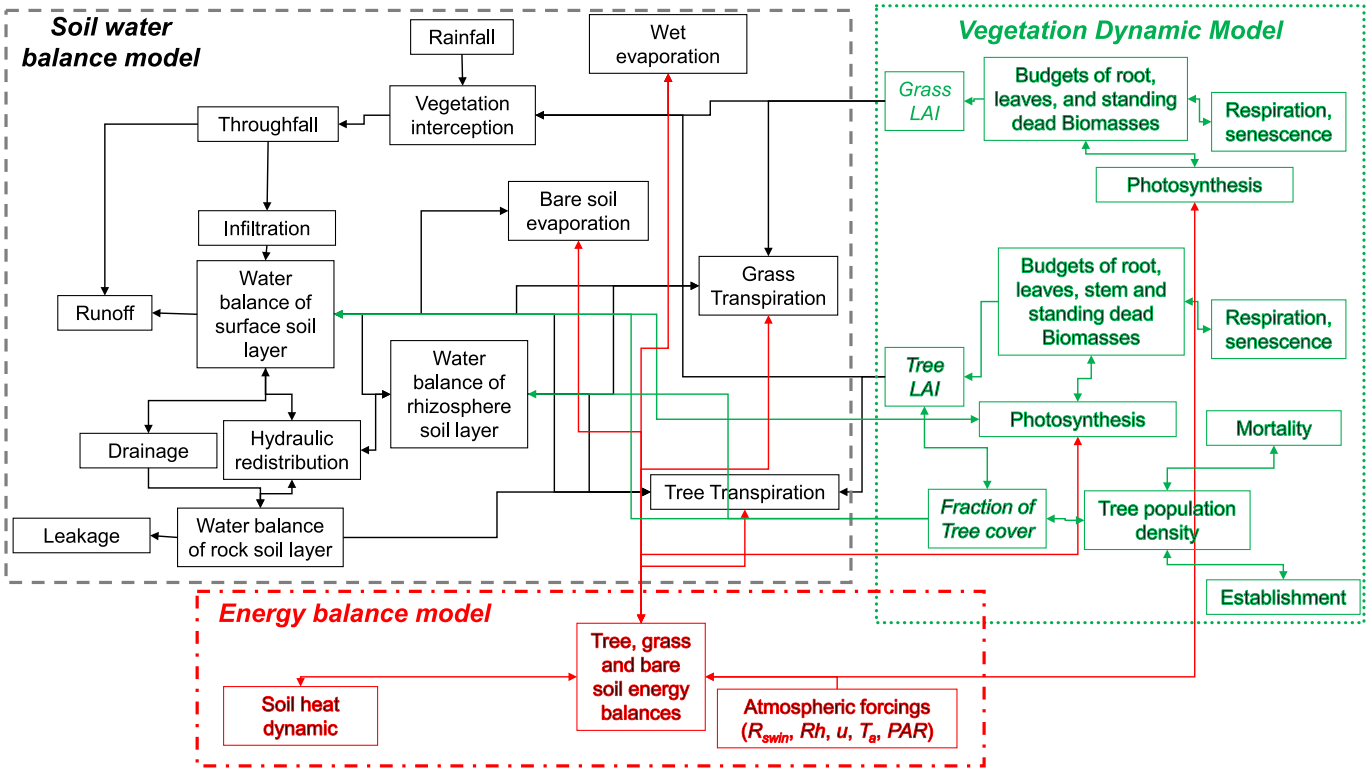

Fig. 1. The proposed ecohydrological model structure with the three main components, soil water balance, energy balance and vegetation dynamic (LAI: leaf area index; R_{swin}: shortwave incoming radiation; Rh: relative humidity; u: wind velocity; T_a: air temperature; PAR: photosynthetically active radiation).

Table 1
Model parameters (VDM-LSM model) for the Orroli site.

Parameter	Description	Value	
		grass	WV
LSM-VDM parameters			
$r_{s,min}$ [s m^{-1}]	minimum stomatal resistance	80	500
T_{min} [°K]	minimum temperature	272.15	268.15
T_{opt} [°K]	optimal temperature	295.15	278.15
T_{max} [°K]	maximum temperature	313.15	318.15
$\theta_{lim,sl}$ [–]	limiting soil moisture for vegetation in the bulk surface soil layer	0.18	0.18
$\theta_{wp,rh}$ [–]	wilting point in the rhizosphere volume	0.12	0.13
$\theta_{lim,rh}$ [–]	limiting soil moisture for vegetation in the rhizosphere volume	0.19	0.19
ω [KPa^{-1}]	slope of the f_3 relation	0.6	0.6
$\theta_{wp,fr}$ [–]	wilting point in the underlying fracture rock layer	0.08	
$\theta_{lim,fr}$ [–]	limiting soil moisture for vegetation in the underlying fracture rock layer	0.18	
$\xi_{g,rh}$	fraction of grass root water uptake in the tree root rhizosphere	0.1	
ξ_t	fraction of tree root water uptake from the surface soil layer	0.8	
Only VDM parameters			
c_l [m^2 gDM^{-1}]	Specific leaf areas of the green biomass in growing season	0.01	0.005
c_d [m^2 gDM^{-1}]	Specific leaf areas of the dead biomass	0.001	0.005
k_e [–]	PAR extinction coefficient	0.5	0.5
ξ_a [–]	Parameter controlling allocation to leaves	0.6	0.55
ξ_s [–]	Parameter controlling allocation to stem	0.1	0.1
ξ_r [–]	Parameter controlling allocation to roots	0.4	0.35
Ω [–]	Allocation parameter	0.8	0.8
m_a [d^{-1}]	Maintenance respiration coefficients for aboveground biomass	0.032	0.0019
g_a [–]	Growth respiration coefficients for aboveground biomass	0.32	0.76
m_r [d^{-1}]	maintenance respiration coefficients for root biomass	0.007	0.002
g_r [–]	growth respiration coefficients for root biomass	0.1	0.1
Q_{10} [–]	Temperature coefficient in the respiration process	2.5	1.5
d_a [d^{-1}]	death rate of aboveground biomass	0.023	0.0045
d_r [d^{-1}]	death rate of root biomass	0.005	0.005
k_a [d^{-1}]	rate of standing biomass pushed down	0.01	0.35
Only LSM parameters			
$z_{om,v}$ [m]	Vegetation momentum roughness length	0.05	0.5
$z_{ov,v}$ [m]	Vegetation water vapor roughness length	z_{om}/7.4	z_{om}/2.5
$z_{om,bs}$ [m]	Bare soil momentum roughness length	0.015	
$z_{ov,bs}$ [m]	Bare soil water vapor roughness length	z_{om}/10	
θ_s [–]	saturated soil moisture	0.53	
b [–]	slope of the retention curve	4	
$k_{s,sl}$ [m/s]	saturated hydraulic conductivity in the surficial root zone	5×10^{-6}	
$\lvert\psi_s\rvert$ [m]	air entry suction head	0.70	
$k_{s,fr}$ [m/s]	saturated hydraulic conductivity in the active fractured rock	5×10^{-4}	
b_{rh} [–]	slope of the retention curve in the tree root rhizosphere	5	
C_{rmax} [mm/MPa/h]	maximum root hydraulic conductance of the active root system	1.5×10^{-6}	
ς_R	Empirical parameter in the hydraulic redistribution equation	2	
d_{rh} [m]	depth of the tree root rhizosphere in the surficial root zone	0.014	
d_{sl} [m]	Surficial root zone depth	0.15	
d_{fr} [m]	Root zone depth of the active fractured rock	2	
C_a [m^2]	Crown area	4	
k_{m1}	Empirical parameter of the growth efficiency of (10)	0.29	
k_{m2}	Empirical parameters of the growth efficiency of (10)	0.02	

from the surficial root zone layer and the deep fractured rock layer below the tips of the sinker roots, defining the maximum depth of the physiologically relevant rock strata (Table 2). Montaldo and Oren (2022) included HR (Table 2), which can be both downward and upward depending on the soil water potential gradient between the surface and deep layers.

Infiltration is estimated using an infiltration excess mechanism (Montaldo et al., 2008) based on the Philip's infiltration equation (Philip, 1957). In the unsaturated soil the Clapp and Hornberger (1978) relationships are used to describe the non-linear dependencies of volumetric soil moisture and hydraulic conductivity (k) on the matric potential (ψ). The evapotranspiration, ET, is given by the sum of the four evapotranspiration components, bare soil evaporation, tree transpiration (which is given by the sum of $E_{t,rh}$ and $E_{t,fr}$), grass transpiration (which is given by the sum of $E_{g,rh}$ and $E_{g,nrh}$), and wet canopy evaporation. As in the original Noilhan and Planton (1989) model, the throughfall rate is modeled through a balance equation of the intercepted water by the canopy reservoir (its capacity is a function of the LAI), which produces throughfall when the reservoir is saturated. E_w was set to the rainfall interception (Noilhan and Planton, 1989). $E_{t,rh}$, $E_{t,fr}$, $E_{g,rh}$, and $E_{g,nrh}$ are estimated based on the Penman-Monteith equation (Brutsaert, 1982; Montaldo et al., 2008) for each plant functional type (PFT, e.g., tree and grass). The canopy resistance, r_c, accounting for environmental stresses, is estimated following Montaldo et al. (2008) for each PFT, using a typical Jarvis (1976) approach (Table 2).

The aerodynamic resistances are estimated as a function of wind velocity through the transfer coefficient for water vapor, C_E (Garratt, 1999), according to the Monin-Obukhov similarity theory. C_E and the heat transfer coefficient (C_H, used in sensible heat flux estimates) account for atmosphere stability (Garratt, 1999), with the flux profile functions for stable and unstable conditions (Garratt, 1999; Montaldo et al., 2008).

Finally, the actual rate of bare soil evaporation is determined as a function of the potential evaporation through a $\alpha(\theta_{sl})$ rate-limiting function (Parlange et al., 1999; Montaldo et al., 2008).

The state of the surface temperature is estimated through the force-restore method (Noilhan and Planton, 1989; Montaldo and Albertson, 2001). Equations for surface temperature and three components (sensible heat flux, H, soil heat flux, G, and the net radiation, R_n) of the energy balance are the same as Noilhan and Planton (1989) and are reported in Table 2. They are applied separately for each land cover component (i.e., seasonal grass patches, evergreen tree clumps, and bare soil), so that the model predicts the energy balance distinctly for each land cover component.

2.1.2. The vegetation dynamic model

The VDM computes change in biomass over time from the difference between the rates of biomass production (photosynthesis) and loss, such as occur through respiration and senescence (e.g., Larcher, 1995; Cayrol et al., 2000). The VDM distinguishes woody vegetation (WV) and grass components and is derived by Montaldo et al. (2005, 2008) from the Nouvellon et al. (2000) model.

In the VDM of WV, four separate biomass states (compartments) are tracked (green leaves, stems, living roots, and standing dead), while the VDM of grass cover distinguishes only three of these biomass compartments: green leaves (B_l), roots, and senesced aboveground components. The biomass [g DM m^{-2}] components are simulated using the approach of Montaldo et al. (2005), which consists of a balance between biomass production (related to photosynthesis for green leaf, stem and root biomass) and biomass destruction (respiration and senescence for green leaf, stem and root biomass), through ordinary differential equations, integrated numerically at a daily time step (Montaldo et al., 2008). The model equations are given in Table 3 and the parameters are presented in Table 1.

The key term of the VDM, photosynthesis, P_g, is computed using the approach of Montaldo et al. (2005), which includes canopy resistance,

Table 2
Equations of the land surface model (LSM) for drainage (D_r), leakage from the fractured rock sublayer below a plane marking the depth of sinker root (L_e), hydraulic redistribution (HR), sensible heat flux (H), net radiation (R_n), soil heat flux (G), surface temperature (T_s), and canopy resistance (r_c). Parameters are defined in Table 1.

Equations
Drainage
$D_r = k_{s,sl}\left(\frac{\theta_{sl}}{\theta_s}\right)^{2b+3}$
$L_e = k_{s,fr}\left(\frac{\theta_{fr}}{\theta_s}\right)^{2b+3}$
Hydraulic redistribution
$HR = R_e C_{rmax}(\psi_{fr} - \psi_{rh}) f_{v,t} D_{tran}$
with $R_e = \frac{1}{1 + \frac{max(\psi_{fr}, \psi_{rh})^{\zeta_R}}{\psi_{50}}}$
Canopy resistance
$r_c = \frac{r_{s,min}}{LAI[f_1(\theta) f_2(T_a) f_3(VPD) f_4(R_{swin})]^{-1}}$
where $r_{s,\min}$ is the minimum stomatal resistance
$f_1(\theta) = \begin{cases} 0 & if \theta \le \theta_{wp} \\ \frac{\theta - \theta_{wp}}{\theta_{lim} - \theta_{wp}} & if \theta_{wp} < \theta < \theta_{lim} \\ 1 & if \theta \ge \theta_{lim} \end{cases}$
$f_2(T_a) = \begin{cases} 0 & \text{for } T_a \leqslant T_{a,\min} \text{ and } T_a > T_{a,\max} \\ 1 - \frac{T_{a,opt} - T_a}{T_{a,opt} - T_{a,\min}} & \text{for } T_{a,\min} < T_a < T_{a,opt} \\ 1 & \text{for } T_{a,opt} \leqslant T_a \leqslant T_{a,\max} \end{cases}$
$f_3(VPD) = 1 - \omega \log(VPD)$
$f_4(R_{swin}) = \frac{R_{swin}(1000 + k_p)}{1000(R_{swin} + k_p)}$
where R_{swin} is the shortwave incoming radiation and k_p equals 1 W/m^2 (Li et al., 2013)
Sensible heat flux
$H = \rho_a c_p C_H u(T_s - T_a)$,
with C_H the heat transfer coefficient
Net radiation
$R_n = R_{swin}(1 - \alpha) + \varepsilon(R_{lwin} - \sigma T_s^4)$,
with R_{swin}, and longwave incoming ration, R_{lwin}, estimated based on equation 6.10 of Brutsaert (1982), α albedo, ε emissivity and σ the Stefan-Boltzmann constant
Soil heat flux
$G = R_n$-H-LE
Surface temperature
$\frac{dT_s}{dt} = C_T G - \frac{2\pi}{\tau}(T_s - T_a)$,
with T_2 the mean T_s value over one day τ, and C_T the soil thermal coefficient
$\frac{dT_2}{dt} = \frac{1}{\tau}(T_s - T_2)$

Table 3
Equations of the vegetation dynamic model components.

Ecophysiological term	Equations
Biomass budget	$\frac{dB_l}{dt} = a_a P_g - R_g - S_g \frac{dB_s}{dt} = a_s P_g - R_s - S_s \frac{dB_r}{dt} = a_r P_g - R_r - S_r \frac{dB_d}{dt} = S_g - L_a$
Photosynthesis	$P_g = \varepsilon_P(PAR) f_{PAR} PAR \frac{1.37 r_a + 1.6 r_{c,\min}}{1.37 r_a + 1.6 r_c}$
	$\varepsilon_P(PAR) = a_0 + a_1 PAR + a_2 PAR^2$
	$f_{PAR} = 1 - e^{-k_e LAI}$
Allocation	For the tree cover:
	$a_a = \frac{\xi_a}{1 + \Omega[2 - \lambda - f_1(\theta)]}$
	$a_s = \frac{\xi_s + \Omega(1 - \lambda)}{1 + \Omega[2 - \lambda - f_1(\theta)]}$
	$a_r = \frac{\xi_r + \Omega(1 - f_1(\theta))}{1 + \Omega[2 - \lambda - f_1(\theta)]}$
	$\xi_a + \xi_s + \xi_r = 1; \lambda = e^{-k_e LAI}$
	For grass cover:
	$a_a = \frac{\xi_a + \Omega\lambda}{1 + \Omega[1 + \lambda - f_1(\theta)]}$
	$a_r = \frac{\xi_r + \Omega(1 - f_1(\theta))}{1 + \Omega[1 + \lambda - f_1(\theta)]}$
	$\xi_a + \xi_r = 1$
Respiration	$R_l = m_a f_4(T) B_l + g_a a_a P_g R_s = m_s f_4(T) B_l + g_s a_s P_g R_r = m_r f_4(T) B_r + g_r a_r P_g f_4(T) = Q_{10}^{\frac{T_m}{10}}$ with T_m = mean daily temperature
Senescence	$S_l = d_a B_l S_s = d_s B_s S_r = d_r B_r$
Litterfall	$L_a = k_a B_d$

linking P_g to soil moisture. Hence, P_g accounts for the contributions of two water sources, the surface root zone and the fractured-rock sublayer down to the reach of tree roots.

The leaf area index is estimated from tree biomass by a linear relationship (Hanson et al., 1988; Nouvellon et al., 2000; Arora, 2003; Montaldo et al., 2005):

$$LAI = c_l B_l \tag{4}$$

where c_l is the specific leaf area of the green biomass.

In this updated version of the model, we included the modeling of the fraction of tree cover dynamics yearly. We related the fraction of individual tree cover to tree LAI ($LAI_{t,ind}$) through a typical Lambert-Beer law (Sitch et al., 2003):

$$f_{t,ind} = 1 - e^{-0.5 LAI_{t,ind}} \tag{5}$$

The reference spatial domain is treated as a mosaic divided into fractional coverages of tree, grass, and bare soil. The overall fraction of tree cover (f_t) in the reference spatial domain is obtained from the average individual fraction of tree cover with the crown area (C_a) and the population density (P_D) through (Sitch et al., 2003):

$$f_t = C_a P_D f_{t,ind} \tag{6}$$

The population density evolves at a yearly time scale (Sitch et al., 2003), through:

$$\frac{dP_D}{dt} = est - mort P_D \tag{7}$$

where *est* is the establishment of new tree individuals each year, available space permitting, and *mort* is yearly tree mortality. The establishment is given by:

$$est = 0.5\left[e^{-7\left(1-f_{t,ind}\right)}\right]\left(1 - f_{t,ind}\right) \tag{8}$$

The mortality is due to low growth efficiency ($mort_{ge}$) and heat stress ($mort_h$) (Sitch et al., 2003; Levis and Bonan, 2004):

$$mort = mort_{ge} + mort_h \tag{9}$$

$$mort_{ge} = \frac{k_{m1}}{1 + k_{m2} g_{eff}} \tag{10}$$

$$mort_h = \frac{GDD_{23^\circ C}}{300} \tag{11}$$

where k_{m1} and k_{m2} are two parameters of growth efficiency, g_{eff} is the growth efficiency, $GDD_{23^\circ C}$ is the annual growing degree days above 23 °C, and $0 \leq mort \leq 1$. Background mortality is estimated by the year growth efficiency as the ratio of the year's biomass increment to leaf area (Sitch et al., 2003; Levis and Bonan, 2004):

$$g_{eff} = \frac{\Delta B_l}{B_l c_l} \tag{12}$$

$GDD_{23^\circ C}$ is estimated using the 10-day running mean of the air temperature (T_{10d}) (Sitch et al., 2003; Levis and Bonan, 2004) as the annual accumulated sum of T_{10d} above a tree specific temperature of 23 °C:

$$GDD_{23^\circ C} = \sum_d (T_{10d} - 23) \tag{13}$$

Note that we are not considering fire occurrence and effects on mortality in this analysis.

The VDM provides estimates of daily values of leaf biomass and, thus, *LAI* of trees and grasses, and yearly values of f_t in turn used by the LSM to estimate evapotranspiration, energy flux, rainfall interception, and soil water content at a half-hour time step. The LSM provides soil moisture and aerodynamic resistances to the VDM.

2.2. The Sardinia case study and the hydrologic database

The Orroli field site is located in east-central Sardinia (39° 41′ 12. 57″ N, 9° 16′ 30. 34″ E, 500 m a. s. L.; details in Detto et al., 2006; Montaldo et al., 2008; Montaldo et al., 2013; Montaldo et al., 2020), where an eddy covariance-based micrometeorological tower was installed in May 2003. The landscape is a patchy mixture of primarily wild-olive tree clumps forming canopy cover over ~33 % of the tower footprint area, ~1.5 km^2 on a gently sloping (~3° from NW to SE) plateau, while interclump zones are covered by herbaceous and grass species during high moisture periods, becoming dry bare soil surface during the rainless summer months. The dominant trees species is wild olive in patches ranging in height from 3.5 to 4.5 m.

The climate at the flux site is maritime Mediterranean, with a mean annual precipitation (1922–2022) of 686 mm (historical precipitation data from a nearby station at 4 km). Mean annual air temperature (T_a) is 15.3 °C, with mean July T_a of 24.5 °C. The soil ranges from 0 to 50 cm in depth, averaging 17 cm ± 6 cm (standard deviation, SD) above a fractured basalt, thus quickly plunging into water-limited conditions during the rainless summer (Detto et al., 2006; Montaldo et al., 2008). The soil is silt loam (19 % sand, 76 % silt, 5 % clay) with a bulk density of 1.38 g/cm^3, and a porosity of 53 %.

2.2.1. Land surface flux data

Extended monitoring was carried out from May 2003 to April 2023, during which micrometeorological, soil moisture, and vegetation dynamics measurements were conducted. Three-dimensional time series sampling of wind velocity, temperature, and CO_2 and water vapor concentration at 10 Hz were averaged over 30 min intervals. These data were used to estimate *ET* and sensible heat flux based on the standard eddy-covariance method (Baldocchi, 2003). The measurements were made with a Campbell Scientific CSAT-3 tri-axial sonic anemometer, and a Licor-7500 CO_2/H_2O infrared gas analyzer, positioned adjacent to each other at the top of the 10 m tall tower. The effect of the gentle slope of the plateau was removed by utilizing the conventional planar fit method, and the Webb-Pearman-Leuning adjustment was applied (Detto et al., 2006).

A Vaisala HMP45 sensor was used to measure T_a and relative humidity (*Rh*). Two infrared transducers, IRTS-P (Apogee Instrument, accuracy of 0.3 °C) were used to measure the surface temperature (T_s [°C]) of the different land cover components. The incoming and outgoing shortwave and longwave radiation components, were measured with a CNR-1 (Kipp & Zonen) integral radiometer with a hemispherical field of view, positioned at 10 m. The photosynthetically active radiation (*PAR* [mmol m^{-2} d^{-1}]) was measured with a LI-190 Quantum Sensor (Licor). Soil heat flux was measured at two different locations close to the tower, one in an open patch (4 m from the tower) and one under a canopy of wild olive trees (5.5 m from the tower), with thermopile plates, HFT3 (REBS), buried at 8 cm below the soil surface. Seven frequency domain reflectometer probes (FDR, Campbell Scientific Model CS-616) estimated soil moisture (Montaldo et al., 2008). Sap flow was monitored using Granier-type heat dissipation sensors (Granier, 1987; Montaldo and Oren, 2022), and data were stored on three CR3000 dataloggers (Campbell Scientific, Logan, UT, USA) at a 30 min time resolution. Sap flux was measured from September 2011 to August 2018, and from July 2021 to September 2021. LAI was measured indirectly through a ceptometer (Accupar model PAR-80, Decagon Devices Inc., Washington USA). LAI measurements were performed mainly during the grass growth season (Montaldo et al., 2008). Finally, specific leaf areas (LAI divided by dry biomass) of predominant grass (=0.01 m^2 gDM^{-1}) and woody vegetation (=0.005 m^2 gDM^{-1}) species were measured directly (by weighing the dry biomass).

For a historical meteorological analysis, daily precipitation from 1922 was available from two nearby rain-gauge stations, Nurri and Villanova Tulo (located < 10 km from the eddy covariance tower, always in the Sarcidano area). We considered mean precipitations of the

two stations, which are correlated with the precipitation (P) at the Orroli station during the overlapping period of operation (correlation coefficient 0.90, $p < 0.001$; slope of 1.08 and intercept of 0.41 mm/d of the linear interpolation with Orroli P). Historical daily air temperatures from 1925 were also available from another nearby station, Mandas (~12 km from the eddy covariance station; correlation coefficient of 0.97, $p < 0.01$, slope of 0.91, and intercept of 2.24 °C of the linear interpolation with Orroli T_a). Historical data of relative humidity, wind velocity and incoming solar radiation were collected from ERA5 European Centre for Medium-Range Weather Forecasts (ECMWF) atmospheric reanalysis datasets (Hersbach et al., 2018; 2020). We used data from 1983, which were successfully validated using 13 years of data of wind velocity at the Orroli station (RMSE = 1 m/s), 13 years of incoming solar radiation data at the Orroli station (RMSE = 35 W/m^2), and 5 years of data of relative humidity at the Orroli station (RMSE = 10 %).

2.2.2. Remote sensing data

A total of 628 remote sensing images were acquired (see Fig. 2) for the 1983–2022 period, from which NDVI was derived at a 30 m spatial resolution. Images from Landsat 5 and 8 were used. For Landsat 5 and 8 the L1TP product was used (it is radiometrically calibrated and orthorectified using ground control points and a digital elevation model to correct for terrain and view angles). The relationship between NDVI and LAI was estimated using simultaneous NDVI data from remote sensors and LAI observations in the field (a total of 37 simultaneous days) ($LAI = \beta_1 + \beta_2 NDVI^{\beta_3}$, with $\beta_1 = -0.435$, $\beta_2 = 1.014$ and $\beta_3 = 0.4029$ for grass in the fall-winter period, $\beta_1 = -0.141$, $\beta_2 = 1.720$ and $\beta_3 = 1.674$ for grass in the spring-summer period, $\beta_1 = 0$, $\beta_2 = 5.392$, and $\beta_3 = 0.486$ for trees).

Furthermore, the aerial photography of 1954, 1978, 2006, 2010, 2013, and 2016 years was available and acquired from the Sardinian Regional photography archive.

A relationship between f_t and NDVI in the field was also estimated using simultaneous NDVI data from remote sensors and f_t estimates from the aerial photography (opportunely classified and processed, and using only data from July and August, when trees are the only vegetation components that survive the dry conditions of the summer season at the Orroli site; $f_t = -0.007579 NDVI^{-2.13} + 0.3313$, rmse = 0.014).

2.3. Future climate scenarios

For future climate scenarios, we considered the IPCC scenarios in the Sixth Assessment report (Swart et al., 2019). We selected eleven Global Climate Models (GCMs) for future scenarios of high, mid and low emissions (CNRM-CM6-1-ssp-245, CNRM-CM6-1-ssp-585, EC-Earth3-CC-585, EC-Earth-AerChem-370, Hadgem3-ll-126, Hadgem3-ll-245, Hadgem3-ll-585, Hadgem3-mm 585, Mpi-esm1-2lr-sf-126, Mpi-esm1-2r-sf370, Mpi-esm1-2r-sf585) that provide complete datasets of precipitation, relative humidity, wind velocity and incoming solar radiation.

Future climate scenarios are generated up to 2100 for the Orroli site from the eleven GCM predictions through the multivariate bias correction technique (Cannon, 2018), which uses the land-observed meteorological data of the past to estimate the required statistics. The reference period is from 2000 to 2014. The multivariate bias correction technique uses an iterative algorithm that consists of three main steps: 1) constructing an uniformly distributed random orthogonal rotation matrix and applying that to the land-observed meteorological target data and to the GCM meteorological source data of the past, 2) correcting the

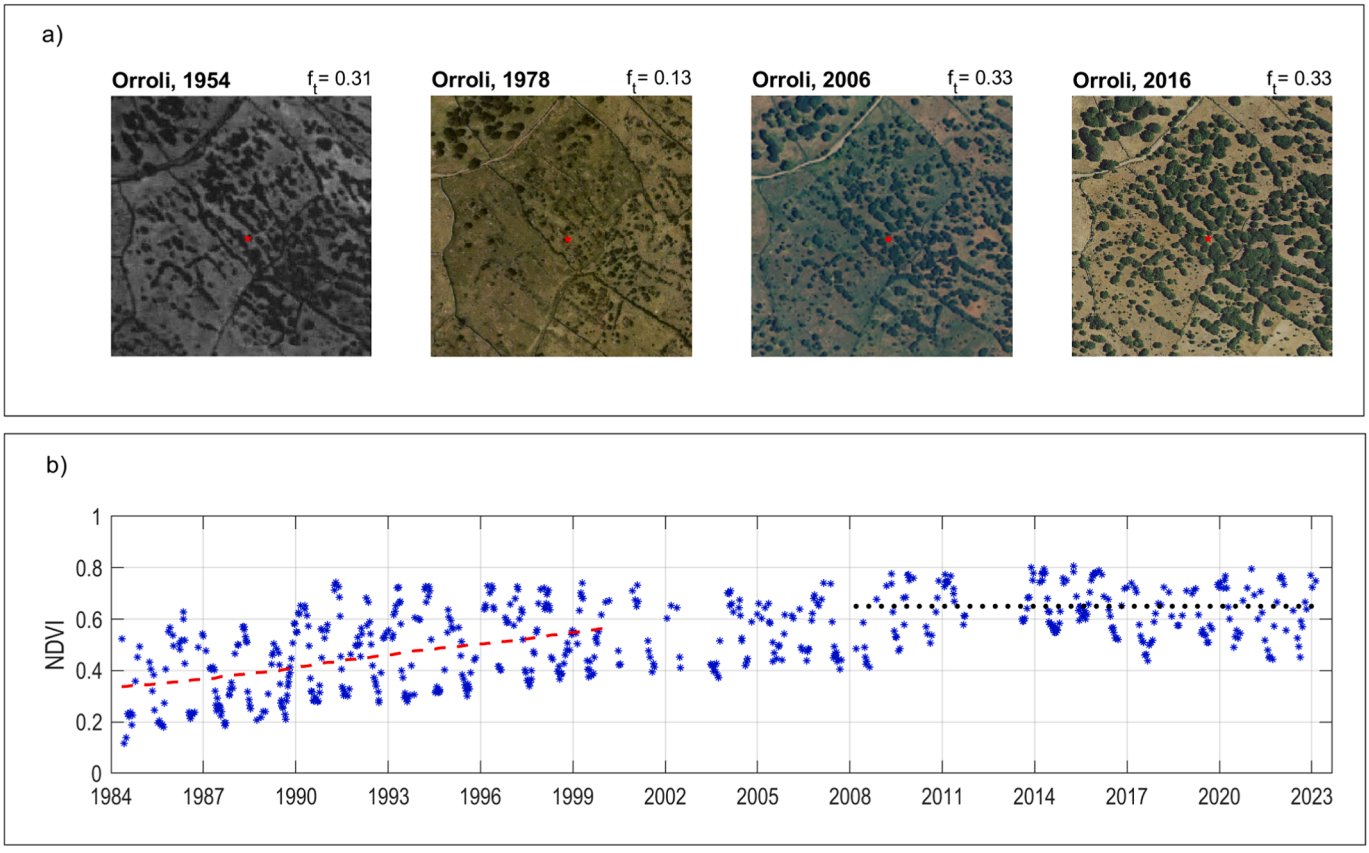

Fig. 2. a) Four historical aerial photographs (in red inside the photograph the position of the tower, and on the top right the estimated fraction of tree cover, f_t), compared with b) the historical evolution of the NDVI at the Orroli site (the positive trend line is in red dashed, Mann Kendal τ of 0.3 and $p < 0.001$, the β slope of the trend line is 0.01/y; the black dotted line represents the constant mean annual NDVI value in last 15 years). (For interpretation of the references to colour in this figure legend, the reader is referred to the web version of this article.)

marginal distributions of the rotated source data by using an empirical quintile map, and 3) applying the inverse rotation to the resulting data. These steps are repeated until the multivariate distribution converges to the target distribution. The multivariate bias correction allowed us to statistically downscale GCM data at the resolution of 1.25° latitude and 1.87° longitude (~150 km) at the Orroli site.

2.4. Comparisons and statistical data analysis

Data were analyzed at hourly, daily, monthly, seasonal and yearly time scales. For annual computations, we used the hydrologic year beginning in Sardinia in September, the end of a typical dry summer (Montaldo and Sarigu, 2017). An index of wetness (*P/PE*, precipitation/potential evaporation) was used to distinguish seasonal meteorological conditions.

Trends of hydrological data (e.g., precipitation and air temperature) were computed using the Mann-Kendall non-parametric test (Kendall, 1938; Sneyers, 1990; Helsel et al., 2020). The Mann-Kendall τ measures the monotonic relationship between two variables, and it is less sensitive to outliers and missing data values. The Theil-Sen slope method was used to estimate the slope linear trends (Theil, 1950; Sen, 1968). Generally, this estimator is frequently applied in climatology and for the analysis of the hydrometeorological time series (Hirsch et al., 1982; Mohsin and Gough, 2010; Hu et al., 2012; Amirabadizadeh et al., 2015) to define the rate of change, β. The Theil-Sen method and the Mann-Kendall test are strongly connected, with the β slope estimator related to the Mann-Kendall τ test statistic (Montaldo and Sarigu, 2017).

Model goodness-of-fit was evaluated by comparing the model results with observations and using the following statistics: mean (μ), standard deviation (SD), mean error, root mean square error (rmse), the coefficient of determination (R^2). ratio of the sums, and mean ratio (R_μ). A sensitivity analysis of model response to parameter values was also performed, assigning a range of realistic values to each parameter to represent the uncertainty of parameter estimates.

3. Results

3.1. Historical data analysis

The availability of historical aerial photography images of the investigated area from 1954 allowed us to evaluate the interesting evolution of land cover (Fig. 2). The spatial distribution of trees in the ecosystem almost 70 years ago was similar with the most recent (Fig. 2), with a f_t of about 0.31 in 1954, and 0.33 in 2006 and 2016. Instead, the aerial photography image of 1978 indicates that tree cover reduced drastically (f_t of about 0.13), due to a human-induced fire in the early seventies. NDVI data, available from the early eighties, showed that tree cover regrew, and the ecosystem naturally responded to the fire disturbance, with a systematic increase of NVDI up to the 2000s (Mann Kendall τ of 0.30, $p < 0.001$) when the vegetation reached almost asymptotically an equilibrium constant value of NDVI of on average ≈0.6 (ranging from 0.4 to 0.8, due to seasonal vegetation growth).

Despite the interannual variability of yearly precipitation from 1922, a significant negative trend (Mann Kendall τ of −0.17, $p = 0.01$) was detected, amplified when looking at winter precipitation (Mann Kendall τ of −0.20, $p = 0.001$; Fig. 3a). At the same time a positive trend of the mean yearly air temperature (Mann Kendall τ of 0.33, $p < 0.001$) from 1925 (Fig. 3b), shows the warming conditions in the last century (~+2 °C). Focusing to the last 4 decades (when NDVI data are also available; Fig. 2), the trend of winter precipitation is not statistically significant, while the trend of yearly air temperature is still significantly positive (Mann Kendall τ of 0.30 and $p < 0.001$; Fig. 3).

3.2. Model calibration and validation

The proposed model correctly predicted soil moisture (rmse = 0.06,

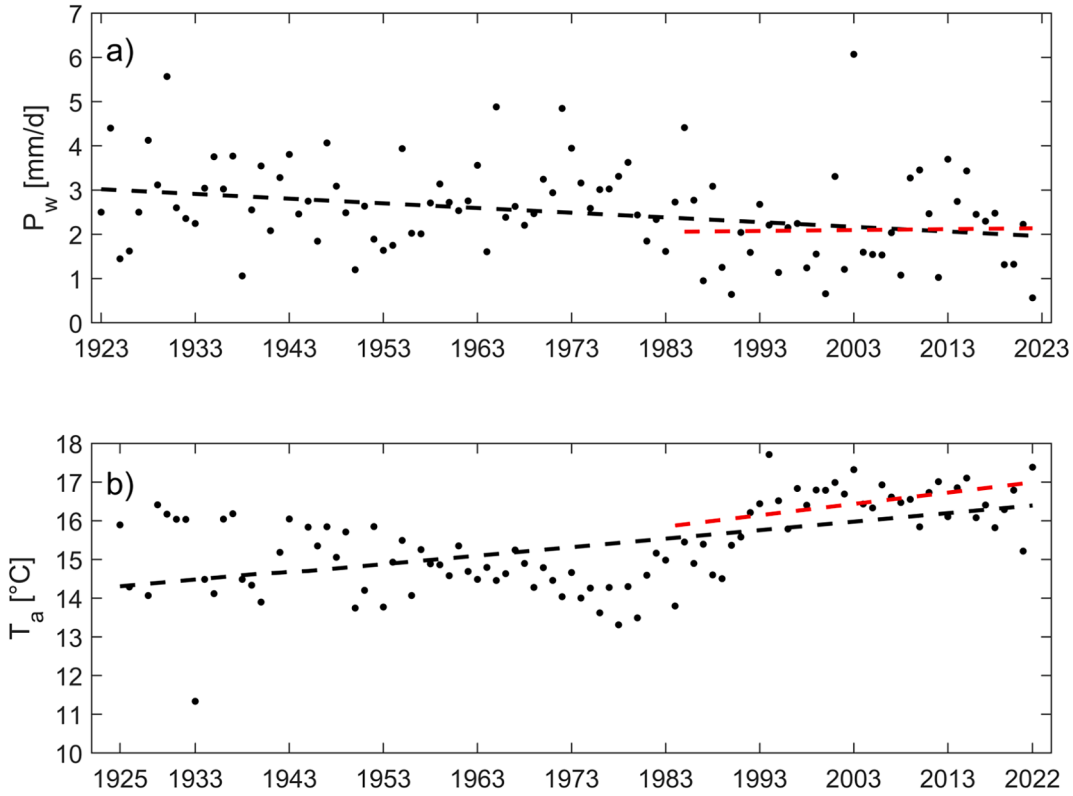

Fig. 3. Historical a) winter precipitation (P_w) and b) annual air temperature (T_a) data, with trend lines of the whole database (black dashed lines) and last 40 years (red dashed lines). (For interpretation of the references to colour in this figure legend, the reader is referred to the web version of this article.)

$R^2 = 0.78$ for the 2003–2013 calibration period, and rmse = 0.06 and $R^2 = 0.74$ for the 2014–2022 validation period; Fig. 4a), and evapotranspiration fluxes [rmse = 0.77 mm/d, ratio of the sums = 0.85 ($R^2 = 0.6$ and $R^2 = 0.73$ for the spring and winter season, respectively) for the 2003–2013 calibration period, and rmse = 0.60 mm/d, ratio of the sums = 0.9, ($R^2 = 0.85$ and $R^2 = 0.83$ for spring and winter season, respectively) for the 2014–2022 validation period; Fig. 4b). Predicted ecosystem ET increased up to the first 2000s, when it reached more constant values (mean ET of 0.85 mm/d for the 1984–1994 period, mean ET of 1 mm/d for the 2003–2013 period, and mean ET of 0.97 mm/d for the 2013–2023 period). The model correctly predicted tree transpiration flux (rmse = 0.29 mm/d; ratio of the sums = 0.88) when compared with tree transpiration estimated from sap flux sensors. The model correctly predicted the increasing trend of f_t from 1983 (Fig. 5a), which stabilized to values of around 0.3–0.35 at the end of the 1990s. The proposed model for f_t predictions [using (6)] was able to represent the increase in tree cover spatial distribution starting from values close to 0.15 in 1983, and reaching its stable conditions with values of f_t around 0.33 in the early 2000s (Fig. 5a), close to those derived from Landsat data (rmse = 0.03, ratio of sums = 0.99, $R^2 = 0.8$ for the 1984–1997 calibration period, and rmse = 0.02, ratio of sums = 0.97, $R^2 = 0.85$ for the 2014–2022 validation period). LAI of tree and grass were also correctly predicted, compared to both tree and grass LAI observations by field data (rmse = 0.25, $R^2 = 0.6$ and rmse = 0.21 $R^2 = 0.69$ for tree and grass species, respectively). We also compared predicted LAI with LAI estimates from Landsat data for the whole period confirming the high performance of the model (rmse = 0.41 for the 1984–1997 calibration period, and rmse = 0.25 for the 2016–2022 validation period, $R^2 = 0.66$ and $p < 0.01$ for the whole period, Fig. 5b). Hydraulic lift was predicted to occur mainly in spring and summer, reaching 0.7–1.0 mm/d in June, from the early 2000s, while it was much lower in the first decade due the low f_t (Fig. 4b).

To verify the robustness of the proposed approach for predicting long term f_t dynamics we tested the model with intentionally different initial conditions of $f_{t,ind}$ and f_t,in comparison with those actually observed: i) equal to the respective values reached in the stable conditions ($f_{t,ind} = 0.85$, and $f_t = 0.33$), and ii) higher than the actual initial conditions ($f_{t,ind} = 0.90$ and $f_t = 0.60$; Fig. 5). In both cases f_t (and $f_{t,ind}$) converged at the end of the 1990s and remained stable and close (≈0.33) to those obtained using the actual initial values, confirming the robustness of the approach (Fig. 5a).

Finally, for evaluating the relative importance of the different parameters for the site, we performed a sensitivity analysis of model response to parameter values (Table 4). A range of realistic values was assigned to each parameter to represent the uncertainty of parameter estimates or measurements (3rd and 9th columns of Table 4). We evaluated the sensitivity of tree and grass biomass, f_t and ET predictions to model parameters. Model responses are sensitive to several grass and tree parameters. Grass and tree biomass predictions are sensitive to most of the corresponding parameters (Table 4). However, grass biomass predictions are sensitive not only to most of the grass parameters (except to $r_{s,\min}$, T_{max}, $\theta_{wp,sl}$, $\theta_{lim,sl}$) but also to some tree parameters (c_d, m_a, g_a and d_a), highlighting the strong interaction between grass and tree.

3.3. Future climate change scenarios

All eleven GCMs predicted future climate change scenarios with increasing air temperature and VPD and decreasing precipitation across the scenario reference periods at the Orroli site, although with different magnitudes (Fig. 6). The worst future climate changes are predicted in the 2076–2100 period, with a decrease of precipitation on average of about 22 % (up to 44 % using EC-Earth3-CC-585), and an increase in air temperature on average of 4.3° C (up to 10.2 °C using CNRM-CM6-1-ssp-585) (Fig. 6). The predicted future increase of air temperature produced an increase of VPD, on average of about 41 % for the 2076–2100 period (up to 75 % using CNRM-CM6-1-ssp-585) (Fig. 6). Lower rises of air temperature (=0.8 °C and 2.3 °C) are predicted using Mpi-esm1-2r-sf126 and Mpi-esm1-2r-sf370 (Fig. 6).

Future climate conditions are used for predictions of the proposed ecohydrologic model. Note that the model results took account of the effect of the increase of CO_2 concentration on plant physiology and biomass production for the future scenarios. In the future scenarios the predicted potential photosynthesis, which is not limited by soil moisture and vapor pressure deficit conditions and directly related to the incoming solar radiation and air temperature conditions, increased 15 %–42 % (mean 24 %) when compared to the historical period, with a positive trend (Mann-Kendall τ of 0.19, $p < 0.01$). The increase of potential photosynthesis is mainly due to the increase of air temperature,

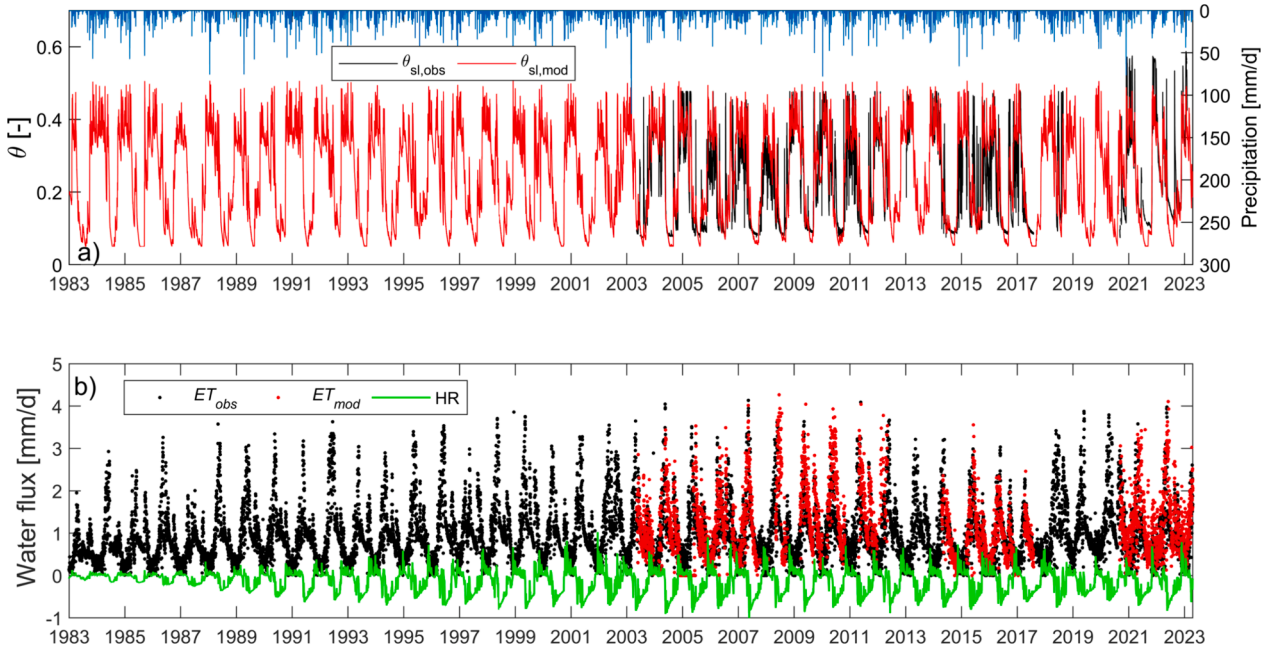

Fig. 4. Observations and model predictions of (a) the soil moisture of the soil layer (θ_{sl}), and b) daily evapotranspiration (ET), and estimated hydraulic redistribution (HR). Negative values of HR represent hydraulic lift while positive values represent hydraulic descent.

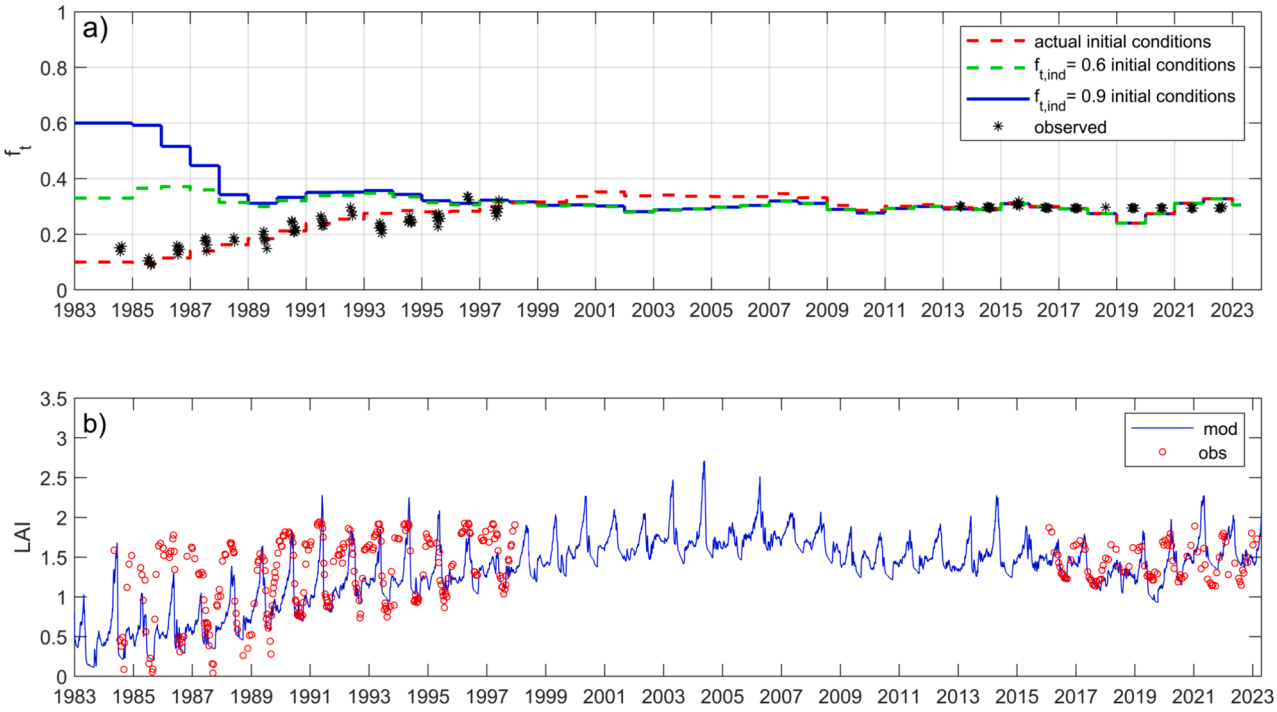

Fig. 5. Using the proposed model at the Orroli site: a) comparison of predicted fraction of tree cover (f_t) with observations derived from remote sensing data; b) comparison of predicted and observed (derived from remote sensing data) ecosystem LAI values.

which positive trend (Mann Kendall τ of 0.20, $p < 0.001$) is similar to that of the potential photosynthesis. Using the EC-Earth3-CC-585 model future climate scenarios, which predicted one of the driest scenarios, the site trees could not survive in the future (Fig. 7), because LAI_t decreased constantly over time; it started from ~4 in 2024, decreased to 2.2 after just 20 years, and further decreased up to 1.4 at the end of the century (Fig. 7). The fraction of tree cover decreased up to 0.3 after 20 years and 0.1 at the end of the century (Fig. 7). Similar decreases are predicted for LAI_t using all the GCM future scenarios, although with a variability of LAI_t at the end of the simulation period (SD = 0.56), ranging from 1.34 (for the Hadgem3_mm585 model) to 3.01 (for the mpi_esm1_2r_sf126 model). On average, at the end of the century LAI_t is predicted at about 2 and f_t at about 0.11 considering all the eleven future scenarios, and LAI_t is predicted at about 1.71 and f_t at about 0.11 for future scenarios of only high and mid emissions. The average LAI_t is predicted to decrease by 46 % when comparing the 2076–2100 period with the historical 2012–2023 period. Considering the 2076–2100 period and future scenarios of high and mid emissions (Table 5), we predicted a strong decrease of infiltration (in average, −25.6 %), which impacts on evapotranspiration (−11.2 %) and tree transpiration in particular (−56.8 %). Interestingly, grass LAI is also predicted to decrease (−26.6 %, Table 5).

Using all eleven GCM predictions, the decrease of tree LAI is strongly related to the decrease of the index of wetness [$\Delta LAI_t = (-4.316\ \Delta P/PE^{-63.12})/(\Delta P/PE\ -21.23)$, $R^2 = 0.90$, $p < 0.001$, Fig. 8.a], which is predicted to decrease up to almost −70 % in the 2076–2100 period producing a decrease of about 2.5 of LAI_t. Using all eleven GCM predictions, the index of wetness decreased for increasing time horizon, and LAI_t systematically decreased (Fig. 8.a).

Considering the worst 25-year future scenario (the 2076–2100 period), HR contributed a larger fraction of tree transpiration seasonally in spring and summer [winter and autumn HR contribution were typically small (Montaldo and Oren, 2022)], increasing with decreasing P/PE [$HR/E_t = -0.9816P/PE^{0.4952} + 0.968$, $R^2 = 0.81$, $p < 0.0001$; Fig. 8.b], becoming particularly high in dry summers ($PE/P < 0.02$) in which HR was 80–90 % of E_t (Fig. 8.b). While HR contributed to a seasonal E_t of 64 % on average for the 2076–2100 period, the contribution was lower in the past monitored period (on average 53 % for the 2003–2023 period). HR contribution to annual E_t was on average 51 %, reaching up to 60 %.

4. Discussion

The attractive long length of the proposed ecohydrological database allowed us to investigate climate and land cover change effects on the Sardinian tree-grass ecosystem. Few large ecohydrological databases with eddy covariance-based data are available, mainly of grass ecosystems, with data from last 20 years (Pang et al., 2021; Yang and Lei, 2022; Zheng et al., 2023). One of the few with a tree-grass ecosystem was in Northern California, where Baldocchi et al. (2021) investigated the annual variability of climate conditions in an oak Savanna ecosystem, characterized by a Mediterranean climate similar to that of the Sardinian ecosystem, using eddy covariance data of almost 20 years. However, the ecosystem was in vegetation stable conditions with the fraction of tree cover not evolving over time. Instead, in the Sardinian case study, the proposed database was longer, and the climate and land cover conditions evolved over the years, making the proposed database very attractive for climate change studies. Although a human-induced fire reset the initial tree cover conditions around 50 years ago, the ecosystem answered naturally and reestablished the equilibrium conditions, almost reaching a constant fraction of tree cover (around 0.33), which was already typical of the ecosystem 70 years ago (Fig. 2). The availability of a such long time series of data of micrometeorological and meteorological measurements, remote sensing data, and aerial photography images provided the opportunity to analyze the response of the tree-grass ecosystem to historical climate and land cover changes. This is a crucial topic for analyzing the past and being able to predict future climate change scenarios.

The proposed model was able to reproduce the soil, vegetation and atmosphere interactions and dynamics, and their long-term evolution. In this proposed version of the model an update was made to account for the coarse time scale (i.e., yearly) dynamics of the tree cover fraction in a

Table 4
Results of the sensitivity analysis of evapotranspiration (ET), fraction of tree cover (ft) and grass and woody vegetation (WV) biomass (B_l) to model parameters (variation range of parameters in the sensitivity analysis and included calibrated value of the parameters) for the Orroli case study. The cells are shaded with gray intensities to reflect four coarse levels of sensitivity in function of the variation (Δ) of the model output (Δ < 6: insensitivity; 2) 6 ≤ Δ < 14: weakly sensitivity; 3) 14 ≤ Δ < 40: sensitivity; 4) Δ ≥ 40: very sensitivity.

Parameter	Woody vegetation						Grass					
	calib.	range	ΔET [%]	Δf_t [%]	ΔB_l WV [%]	ΔB_l grass [%]	calib.	range	ΔET [%]	Δf_t [%]	ΔB_l WV [%]	ΔB_l grass [%]
$r_{s,min}$ [s m^{-1}]	280	200-360	51	84	95	5	80	40-120	20	12	1	6.3
T_{min} [°K]	293.15	290.15-296.15	7	14	6	4.5	272.15	269.15-275.15	5	12	0.17	18
T_{opt} [°K]	324.15	321.15-327.15	38	14	73	4.3	295.15	292.15-298.15	6	12	1	18
T_{max} [°K]	324.15	321.15-327.15	4.8	14	6	4	324.15	321.15-327.15	5	11	1	4
$\theta_{wp,sl}$ [-]	0.18	0.1-0.24	4.2	15	10	0.6	0.10	0.02-0.16	1	12	1.7	13
$\theta_{lim,sl}$ [-]	0.24	0.15-0.3	1.7	14	5	.7	0.18	0.15-0.21	1.5	11	1.9	11
c_l [m^2 gDM^{-1}]	0.005	0.0044-0.0056	35	14	95	6	0.01	0.0095-0.0106	35	12	6.5	96
c_d [m^2 gDM^{-1}]	0.005	0.0044-0.0056	40	15	96	14	0.001	0.00045-0.0016	35	12	6.4	96
m_a [d^{-1}]	0.0003	0.0003-0.0009	69	83	100	96	0.032	0.026-0.038	35	12	6	95
g_a [-]	0.74	0.64-0.84	26	44	62	56	0.27	0.22-0.32	34	14	3.6	87
m_r [d^{-1}]	0.002	0.0015-0.0025	35	15	53	7.5	0.007	0.002-0.012	35	14	6.3	96
g_r [-]	0.1	0.05-0.15	35	15	93	5	0.1	0.05-0.15	31	11	2.6	74
Q_{10} [-]	2	1.5-2.5	21	34	42	12	2.5	2-3	59	13	49	64
d_a [d^{-1}]	0.00051	0.00021-0.00081	40	16	96	37	0.023	0.019-0.027	35	12	6.1	95
d_r [d^{-1}]	0.005	0.002-0.008	35	15	96	6.9	0.005	0.002-0.008	35	12	6.3	96
k_a [d^{-1}]	0.35	0.3-0.4	33	14	83	3.3	0.01	0.005-0.015	36	11	6.3	95
r_x [-]	0.5	0.3-1	25	14	45	1.2	0.8	0.6-1	29	12	1.2	46
$k_{s,sl}$ [m/s]	$5\ 10^{-6}$	$5\ 10^{-8}$- $4\ 10^{-4}$	4.8	13	4.3	4.3						

tree-grass ecosystem. Compared to existing models the proposed model is still simplified with low parameterization and at the same time it is able to reproduce both fine ecophysiological processes at a hourly time scale, like the hydraulic redistribution process and the water uptake of tree roots from below fractured rock, and more coarse processes at yearly time scales like tree cover fraction evolution. Indeed, existing models are more complex, like the global vegetation models (Sitch et al., 2003; Gerten et al., 2004; Reick et al., 2013; Zhu et al., 2015), where vegetation dynamics are modeled using more sophisticated and parameterized approaches and are developed for coarse spatial scales (Song et al., 2013). The proposed model is still simple for parameterization and computational burden but captures vegetation and soil interactions at short and long time scales, allowing good performance for LAI (rmse = 0.21), soil moisture (rmse = 0.06), and evapotranspiration (rmse = 0.7 mm/d) predictions at a local scale. Although a human-induced fire reduced the tree cover of the ecosystem around 50 years ago, the ecosystem restored the tree cover distribution in almost 20 years. The model was able to reproduce this occurrence coarsely, confirming its ability and potential for being used in climate change studies. Other models used a similar approach for long term tree cover evolution (Sitch et al., 2003; Reick et al., 2013), and have been used for simulating future climate change scenario impacts on LAI (Heubes et al., 2011; Hickler et al., 2012; Antúnez et al., 2018), while we validated the proposed approach in detail thanks to the unusual and attractive database, which included the past human-induced fire event and proved model ability and performance for long-term predictions. In our model f_t converged at the end of the 1990s close to the values (≈0.33) observed, and was even insensitive to the initial model conditions, confirming the robustness of the approach. Note that in our approach we are not considering fire occurrence and effects on tree mortality to concentrate the analysis on vegetation and climate relationships, although we recognize that it is an important natural disturbance at a global scale

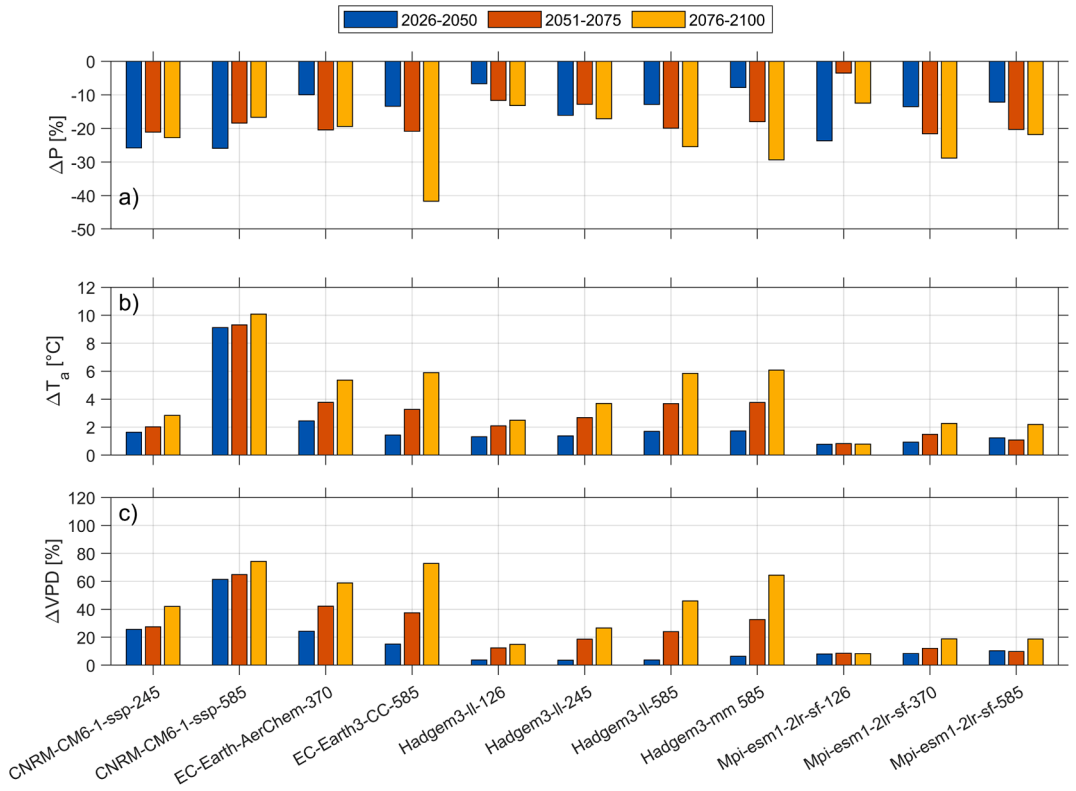

Fig. 6. For the future scenarios, the predicted changes of precipitation (ΔP), air temperature (ΔT_a), and vapor pressure deficit (ΔVPD) at the Orroli case study using the 11 GCMs respect to the past.

(Sitch et al., 2003), and could be considered in our future research at larger spatial scales.

Tree and grass interact and compete for water resources in the water-limited ecosystem. Montaldo et al. (2021) demonstrated that the root system of the wild olives and the hydraulic redistribution between the underlying rocky moisture and the surface soil moisture layer sustain the physiological activity of grass during dry periods at the Orroli tree-grass ecosystem. In the sensitivity analysis of the model response to parameters, grass biomass predictions were sensitive not only to grass parameters but also to tree parameters, highlighting the strong interaction between grass and tree. Following Montaldo et al. (2021), grass LAI and ET fluxes were also reevaluated under a hypothetical scenario in which the pasture grass covers the entire area, and therefore the source of water from rock moisture was not available. Without the tree component, ET is reduced by ~95 % and to ~96 % for the historical and the future climate scenarios, respectively, and LAIg is reduced by 40 % and 38 % for the for the historical and the future climate scenarios, respectively. Hence, water taken up by tree roots from the rocky substratum was key to maintaining stomata open, allowing photosynthesis and, thus, survival and development of not only trees, but also of the seasonal vegetation in the pasture, likely through hydraulic redistribution.

The Mediterranean ecosystem was affected by a historical decrease of winter precipitation (from 1922, Mann Kendall τ of −0.20, $p = 0.001$; Fig. 3), which is a key season for the sustainability of the Sardinian water resources system because typically precipitation is mainly concentrated in that season producing most of the runoff and groundwater recharge (Corona et al., 2018; Montaldo and Oren, 2022). Although the drought conditions were amplified by the increase in air temperature in the last century (Mann Kendall τ of 0.33, $p < 0.001$), the tree cover of the Sardinian ecosystem didn't yet change, remaining similar to that in 1954 ($f_t \approx$ 0.3–0.35; Fig. 2). The mean annual precipitation (MAP) decreased (MAP = 692 mm for the 1922–1954 period, and MAP = 633 mm for the 1992–2022 period), but was still above 600 mm, apparently enough to sustain tree growth, and the tree cover fraction of ≈0.33 (Fig. 9). Indeed, in those conditions the index of wetness was still higher than 0.02 and on average equal to 0.25 (Fig. 8.b). Drier (on average −20 %, up to −42 %) and warmer (on average +4 °C, up to +10.1 °C) climate conditions are predicted by the recent IPCC climate scenarios opportunely rescaled for the Sardinian case study (Fig. 6), consistent with other findings in the Mediterranean area (May, 2008; Ozturk et al., 2015). Wild olive is a common Mediterranean species (Lumaret and Ouazzani, 2001; Terral et al., 2004), extended in the Mediterranean area since the Late Paleogene (Terral et al., 2004). Despite the human-induced fire of 50 years ago, wild olives regrew thanks to the typical climate conditions of the Mediterranean site, and they were able to survive short droughts (e.g., in years 2001, 2012, 2005, and 2017) thanks to their efficient root system. Wild olives develop an adaptation strategy to rely on a range of avoidance and tolerance mechanisms that maintain internal water status and metabolic activity during dry periods (Connor, 2005; Fernandez et al., 1997; Lo Gullo and Salleo, 1988; Ramos and Santos, 2009). This strategy consists of the control of transpiration and water uptake of roots developed in deep soil layers (Nadezhdina et al., 2015). As is typical in Mediterranean basins, wild olives in the Sardinian site expanded their roots into the underlying fractured basalt. In this way, trees can survive dry periods using water infiltrated into fractured rock during previous wet seasons and held in soil pockets (Cannon, 1911; Estrada-Medina et al., 2013; Montaldo et al., 2021; Montaldo and Oren, 2022). Despite their strong resistance to droughts, the predicted future climate change will decrease precipitation further, with MAP decreasing below 600 mm, and up to 380 mm in the 2075–2100 scenario (for the EC-Earth3-CC-585 GCM; Fig. 9). At present, the developed tree cover percentage (~33 %) of the Sardinian site is sustainable with the historical MAP (>600 mm/y). This is also in agreement with Yang et al. (2016) and Axelsson and Hanan (2017), which recently updated Sankaran et al.'s (2005) results and estimated sustainable woody cover percentages for a large range of MAP in African and Texan dry ecosystems (Fig. 9). Instead, with the decrease of MAP for future scenarios, the tree cover fraction will decrease up to less than 10

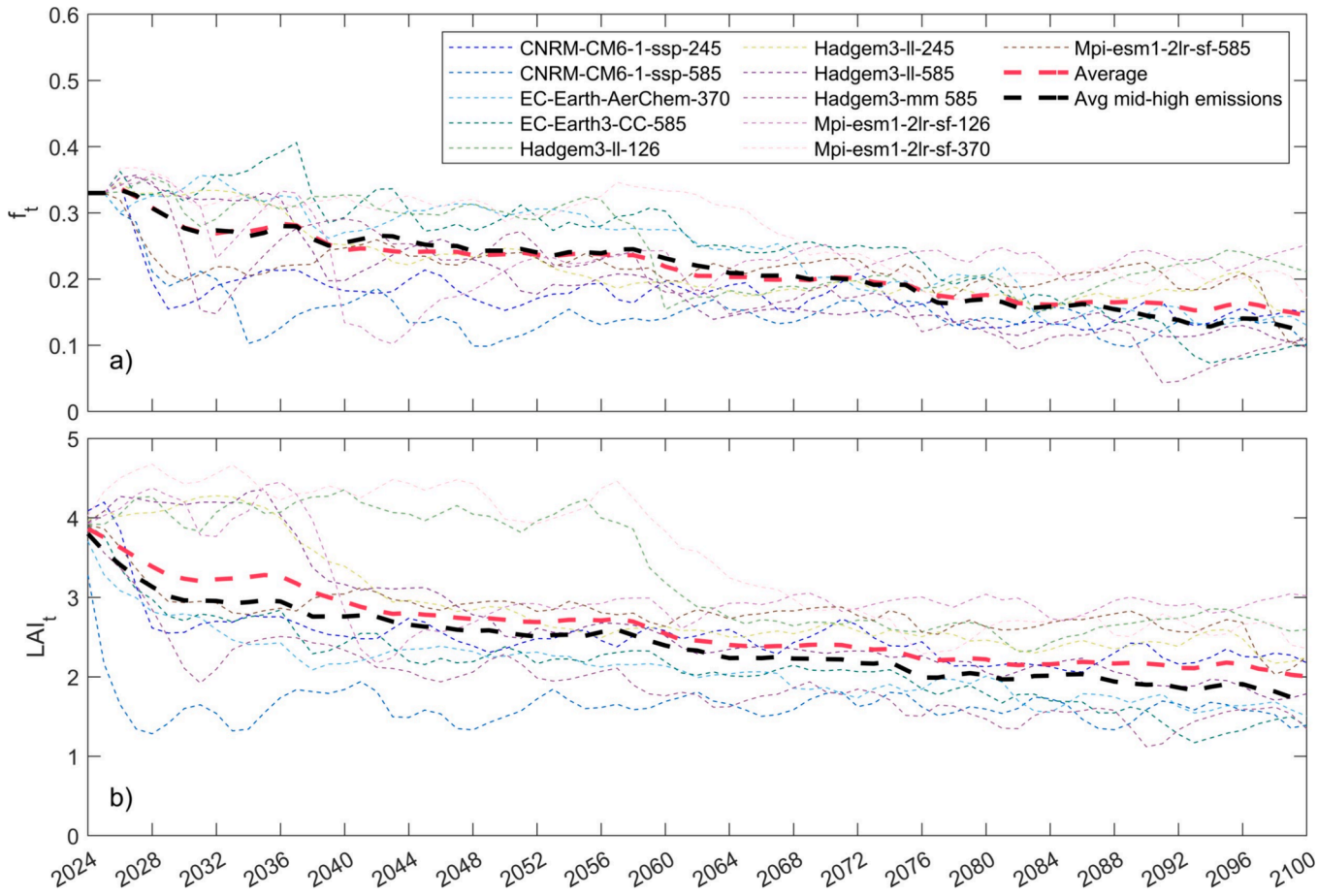

Fig. 7. Future predicted scenarios using the 11 GCMs inputs at the Orroli site: predictions of a) the fraction of tree cover (f_t) and b) the tree LAI (LAI_t). The dashed thick red lines are the averages of the f_t and LAI_t predictions using all the 11 GCMs inputs, and the dashed thick black lines are the averages of the f_t and LAI_t predictions using mild and high emission scenarios only. (For interpretation of the references to colour in this figure legend, the reader is referred to the web version of this article.)

Table 5
Results of the model predictions for the future 2075–2100 scenario and future scenarios of high and mid emissions: mean yearly values, and the corresponding changes compared to the historical data.

Variable name	Mean yearly values (Standard deviation)	Change (2075–2100 respect historical)
Infiltration (I)	391.5 mm/year (SD = 43.75 mm/year)	−25.6 %
Evapotranspiration (ET)	310 mm/year (SD = 27.12 mm/year)	−11.2 %
Tree transpiration (E_t)	68.52 mm/year (SD = 19.86 mm/year)	−68.51 %
Hydraulic redistribution (HR)	35.62 mm/year (SD = 8.655 mm/year)	−37 %
Soil moisture (θ_{sl})	0.19 (SD = 0.02)	−21.7 %
Moisture in the fractured rock layer (θ_{fr})	0.25 (SD = 0.05)	−3.3 %
Tree leaf area index (LAI_t)	1.9 (SD = 0.47)	−52 %
Grass leaf area index (LAI_g)	0.23 (SD = 0.07)	−26.6 %

%. The decrease of f_t with the decrease of MAP below 600–650 mm/y is also in agreement with Yang et al. (2016) and Axelsson and Hanan (2017), which, however, predicted the MAP and f_t relationship using a spatial analysis on recent data (Fig. 9). In our time scale analysis at the local spatial scale, we demonstrated that the predicted future drier conditions would impact the existing tree-grass ecosystem equilibrium, resulting in a drastic decrease in the tree cover.

The increase in air temperature (+4.3 °C on average in the 2075–2100 scenario) with the decrease in the precipitation, enhanced the dry conditions in the future, with a strong decrease of the wetness conditions (P/PE decreased up to −15 % in the 2075–2100 scenario). The predicted decrease of the wetness index will bring to a decrease of the tree LAI of 2.5 (~-60 %; Fig. 8.a), and the tree cover fraction up to 0.1, so that the wild olives would not survive in the Sardinian ecosystem in the predicted future scenarios. As also observed by Montaldo et al. (2021) and Montaldo and Oren (2022), with respect to the highly monitored 2003–2023 period, HR contribution to E_t increased during dry springs and in summers when seasonal P/PE was less than 0.1, reaching the highest values of 80 % of E_t. Such high contribution of HR was also observed by Schwinning (2010) in Mediterranean Jeffrey pine trees. In the predicted future scenarios, the increase of dry conditions with P/PE below 0.005 will increase the HR contribution to E_t, reaching 91 % (Fig. 8.b), which, however, will be not enough to support tree growth and maintenance, evidenced by very low LAI_t (between 1.5 and 2) and f_t (~0.1) values (Fig. 7). In the predicted future conditions, as was similarly observed in the Mediterranean basin by Garcia-Ruiz et al. (2011), in a Turkish basin by Gorguner and Kavvas (2020), and in Sardinian basins by Pulighe et al. (2021) and Sirigu and Montaldo (2022), the soil water balance will be strongly modified, with a decrease of infiltration (−25.6 %), and soil water content (−21.7 %). We also predicted a strong decrease of evapotranspiration (−11.2 %) and tree transpiration (−56.8 %) due to tree cover percentage reduction. In this future scenario, grass LAI will also decrease (on average – 26.6 %) because the hydraulic lift generated by the tree root system supported grass growth in these dryland ecosystems (Montaldo et al., 2021), and

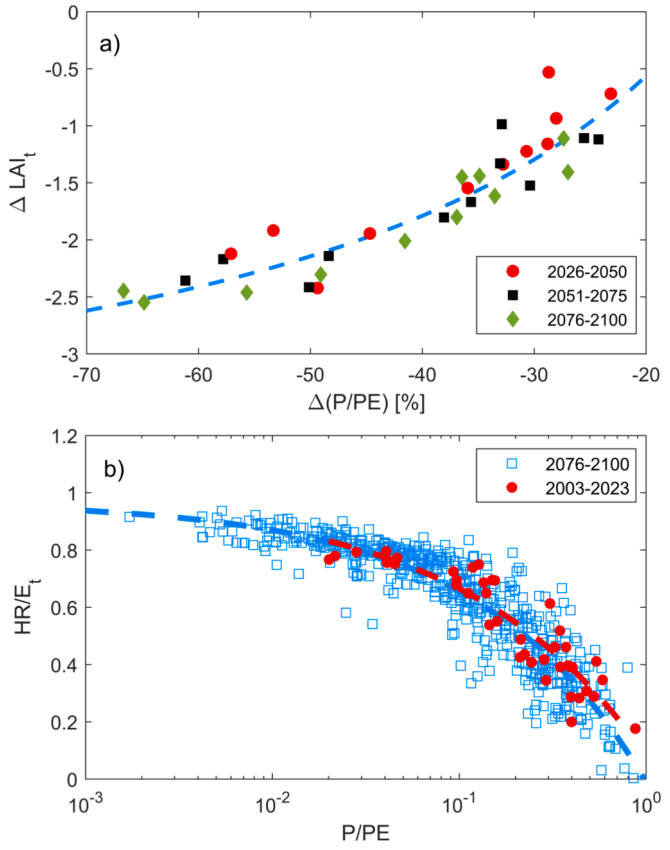

Fig. 8. Using the proposed model and the 11 GCMs inputs: a) changes of mean annual tree LAI (ΔLAI_t) *versus* the variation of the wetness index [Δ (P/PE), P = precipitation, PE = potential evaporation] respect to the past [dash blue line is the regression line with equation: $\Delta LAI_t = (-4.316\ \Delta P/PE^{-63.12})/(\Delta P/PE - 21.23)$, $R^2 = 0.9$] for the future predicted scenarios (2026–2050, 2051–2075, and 2076–2100 periods); b) the spring and summer contributions of the hydraulic redistribution (HR) to the tree transpiration (E_t) *versus* the wetness index (P/PE) for the 2076–2100 scenario [regression lines are for the historical (dash red line: $HR/E_t = -0.9098P/PE^{0.4492} + 0.9883$, $R^2 = 0.84$, $p < 0.001$) and future (dash blue line: $HR/E_t = -0.9816P/PE^{0.4952} + 0.9698$, $R^2 = 0.81$, $p < 0.0001$) periods]. (For interpretation of the references to colour in this figure legend, the reader is referred to the web version of this article.)

the predicted decrease of LAI_t and f_t will cause a decrease of HR (on average −62 %), with consequences on the landscape aspect, becoming more and more a savanna-like ecosystem.

The Sardinian site is characterized by a strong interannual variability of annual precipitation, as typical of the Mediterranean region (Ramos, 2001; Giorgi et al., 2004; Montaldo et al., 2008), and we estimated a lower limit for annual precipitation (~600 mm/y) below which the recharge of rock reservoir during wet months could no longer sustain the tree's water needs during the dry months, jeopardizing the tree's survival in the ecosystem. The drier conditions, such as those predicted using future climate change projections in the Mediterranean area, will impact the existing wild olive – grass ecosystem equilibrium, decreasing the woody cover spatial distribution. For the hydrologic sustainability of a tree-grass ecosystem more water-resistant vegetation species may be planted, or develop naturally, with impacts on a typical environmental landscape of the Mediterranean region.

5. Conclusions

A very attractive long-term database (>60 years of data) of a Sardinian case study, in the center of the island and the Mediterranean Sea, characterized by a tree (wild olive) – grass ecosystem, with

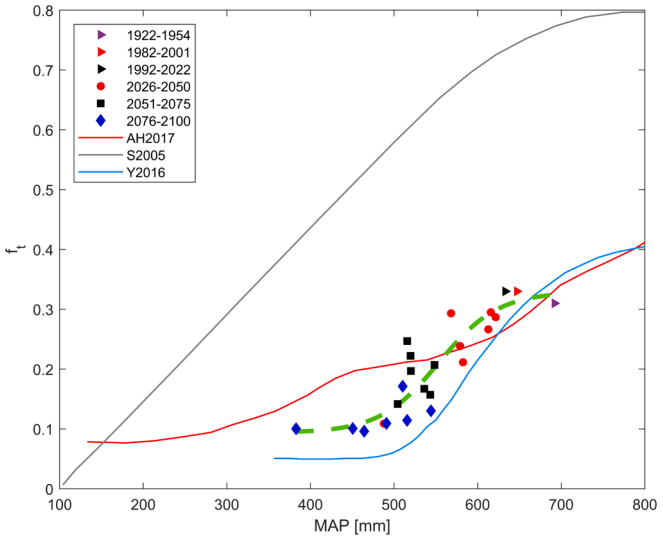

Fig. 9. The historical and future (as predicted using the mild and high emission scenarios) fraction of tree cover (f_t) *versus* the mean annual precipitation (MAP) in the Orroli site (in dash green line the regression line with equation $f_t = 0.0936 + 0.2354/(1 + e^{-(MAP-553.7345)/35.4098})$, $R^2 = 0.81$). For comparison the f_t (MAP) relationships of Sankaran et al. (2005; S2005), Axelsson and Hanan (2017; AH2017), and Yang et al. (2016; Y2016) are reported. (For interpretation of the references to colour in this figure legend, the reader is referred to the web version of this article.)

micrometeorological and meteorological measurements, remote sensing data and aerial photography images, is proposed. We demonstrated that it provided an interesting opportunity to analyze the response of tree-grass ecosystems to historical climate and land cover changes.

An ecohydrological model to accurately reproduce the soil, vegetation, and atmosphere interactions and dynamics, and their long-term evolution is proposed. It predicted the long-term dynamics of the Sardinian tree-grass ecosystem, well predicting the tree cover fraction, which was drastically reduced (~0.10) by a human-induced fire about 50 years ago, and restored naturally in almost 20 years, reaching the equilibrium value (~0.33). Through a statistical analysis of historical precipitation and air temperature data, we evaluated that the Sardinian case study suffered a historically significant reduction of rain and a significant increase of air temperature in the last century, which produced drier conditions but with a recent mean annual precipitation (MAP) still above 600 mm, apparently enough to sustain the tree growth. We predicted future scenarios using the Intergovernmental Panel on Climate Change (IPCC) climate scenarios, opportunely rescaled for the Sardinian case study. A further decrease of MAP of up to ~400 mm, and an increase of air temperature of on average 5.39 °C (up to 10 °C), which will cause a reduction in the tree cover fraction of up to 0.10, and a strong decrease of tree LAI is predicted. In the predicted future scenarios, the wild olives would not survive in the Sardinian ecosystem. The soil is predicted to become drier, with less infiltration, and less grass and vegetation in general, with consequences on the landscape aspect, increasingly becoming more of a savanna-like ecosystem.

The future landscape scenarios are predicted to be less vegetated, unless more water-resistant vegetation species develop naturally or are planted. Water resources and environmental planning need to consider and evaluate these results to develop strategies able to increase the resilience of tree-grass ecosystems to climate changes.

CRediT authorship contribution statement

Nicola Montaldo: Writing – review & editing, Writing – original draft, Visualization, Validation, Supervision, Software, Resources,

Project administration, Methodology, Investigation, Funding acquisition, Formal analysis, Data curation, Conceptualization. **Roberto Corona:** Writing – original draft, Visualization, Validation, Software, Methodology, Formal analysis, Data curation.

Declaration of competing interest

The authors declare that they have no known competing financial interests or personal relationships that could have appeared to influence the work reported in this paper.

Data availability

Data will be made available on request.

Acknowledgements

This work was supported by the Italian Ministry of Education, University and Research (MIUR) through the SWATCH European project of the PRIMA MED program, CUP n. F24D19000010006, the ALTOS European project of PRIMA MED program, CUP n. F24D19000020006, and the FLUXMED European project of the WATER JPI program, CUP n. F24D19000030001. We thank Claudia Chessa for preliminary support to data collection, and ARPAS (the Sardinia regional agency for environmental protection) for providing historical data.

References

Albertson, J.D., Kiely, G., 2001. On the structure of soil moisture time series in the context of land surface models. J. Hydrol. 243 (1–2), 101–119. https://doi.org/10.1016/s0022-1694(00)00405-4.

Amirabadizadeh, M., Huang, Y.F., Lee, T.S., 2015. Recent trends in temperature and precipitation in the Langat River Basin, Malaysia. Adv. Meteorol. 1–16 https://doi.org/10.1155/2015/579437.

Antúnez, P., Suárez-Mota, M.E., Valenzuela-Encinas, C., Ruiz-Aquino, F., 2018. The potential distribution of tree species in three periods of time under a climate change scenario. Forests 9 (10). https://doi.org/10.3390/f9100628.

Arora, V.K., 2003. Simulating energy and carbon fluxes over winter wheat using coupled land surface and terrestrial ecosystem models. Agric. For. Meteorol. 118 (1–2), 21–47.

Axelsson, C.R., Hanan, N.P., 2017. Patterns in woody vegetation structure across African savannas. Biogeosciences 14 (13), 3239–3252. https://doi.org/10.5194/bg-14-3239-2017.

Baldocchi, D.D., 2003. Assessing the eddy covariance technique for evaluating carbon dioxide exchange rates of ecosystems: past, present and future. Glob. Chang. Biol. 9 (4), 479–492. https://doi.org/10.1046/j.1365-2486.2003.00629.x.

Baldocchi, D., Ma, S.Y., Verfaillie, J., 2021. On the inter- and intra-annual variability of ecosystem evapotranspiration and water use efficiency of an oak savanna and annual grassland subjected to booms and busts in rainfall. Glob. Chang. Biol. 27 (2), 359–375. https://doi.org/10.1111/gcb.15414.

Barbeta, A., Ogaya, R., Peñuelas, J., 2013. Dampening effects of long-term experimental drought on growth and mortality rates of a Holm oak forest. Glob. Chang. Biol. 19 (10), 3133–3144.

Breshears, D.D., 2006. The grassland-forest continuum: trends in ecosystem properties for woody plant mosaics? Front. Ecol. Environ. 4 (2), 96–104. https://doi.org/10.1890/1540-9295(2006)004[0096:tgctie]2.0.co;2.

Brutsaert, W., 1982. Evaporation into the Atmosphere: Theory, History, and Applications. Springer, Dordrecht, 299. https://doi.org/10.1007/978-94-017-1497-6.

Cannon, W.A., 1911. The Root Habits of Desert Plants. Carnegie Institution of Washington.

Cannon, A.J., 2018. Multivariate quantile mapping bias correction: an N-dimensional probability density function transform for climate model simulations of multiple variables. Clim. Dyn. 50 (1–2), 31–49. https://doi.org/10.1007/s00382-017-3580-6.

Cayrol, P., et al., 2000. Grassland modeling and monitoring with SPOT-4 VEGETATION instrument during the 1997–1999 SALSA experiment. Agric. For. Meteorol. 105 (1–3), 91–115. https://doi.org/10.1016/s0168-1923(00)00191-x.

Clapp, R.B., Hornberger, G.M., 1978. Empirical equations for some soil hydraulic properties. Water Resour. Res. 14 (4), 601–604.

Clark, P.U., et al., 2016. Consequences of twenty-first-century policy for multi-millennial climate and sea-level change. Nat. Clim. Chang. 6 (4), 360–369. https://doi.org/10.1038/nclimate2923.

Connor, D.J., 2005. Adaptation of olive (Olea europaea L.) to water-limited environments. Aust. J. Agr. Res. 56 (11), 1181–1189. https://doi.org/10.1071/ar05169.

Corona, R., Montaldo, N., Albertson, J.D., 2018. On the role of NAO-driven interannual variability in rainfall seasonality on water resources and hydrologic design in a typical mediterranean basin. J. Hydrometeorol. 19 (3), 485–498. https://doi.org/10.1175/jhm-d-17-0078.1.

D'Odorico, P., Porporato, A., Runyan, C.W., 2019. Dryland Ecohydrol. https://doi.org/10.1007/978-3-030-23269-6.

David, T.S., et al., 2013. Root functioning, tree water use and hydraulic redistribution in Quercus suber trees: a modeling approach based on root sap flow. For. Ecol. Manage. 307, 136–146. https://doi.org/10.1016/j.foreco.2013.07.012.

Detto, M., Montaldo, N., Albertson, J.D., Mancini, M., Katul, G., 2006. Soil moisture and vegetation controls on evapotranspiration in a heterogeneous Mediterranean ecosystem on Sardinia, Italy. Water Resour. Res. 42 (8), 16. https://doi.org/10.1029/2005wr004693.

Domec, J.C., et al., 2010. Hydraulic redistribution of soil water by roots affects whole-stand evapotranspiration and net ecosystem carbon exchange. New Phytol. 187 (1), 171–183. https://doi.org/10.1111/j.1469-8137.2010.03245.x.

Doughty, C.E., et al., 2015. Drought impact on forest carbon dynamics and fluxes in Amazonia. Nature 519 (7541), 78–U140. https://doi.org/10.1038/nature14213.

Eliades, M., et al., 2018. The water balance components of Mediterranean pine trees on a steep mountain slope during two hydrologically contrasting years. J. Hydrol. 562, 712–724. https://doi.org/10.1016/j.jhydrol.2018.05.048.

Estrada-Medina, H., Graham, R.C., Allen, M.F., Jimenez-Osornio, J.J., Robles-Casolco, S., 2013. The importance of limestone bedrock and dissolution karst features on tree root distribution in northern Yucatan. Mexico. Plant and Soil 362 (1–2), 37–50. https://doi.org/10.1007/s11104-012-1175-x.

Fan, Y., Miguez-Macho, G., Jobbágy, E.G., Jackson, R.B., Otero-Casal, C., 2017. Hydrologic regulation of plant rooting depth. Proc. Natl. Acad. Sci. U.S.A. 114(40), 10572–10577. DOI:10.1073/pnas.1712381114.

Fernandes, P.M., 2013. Fire-smart management of forest landscapes in the Mediterranean basin under global change. Landsc. Urban Plan. 110, 175–182. https://doi.org/10.1016/j.landurbplan.2012.10.014.

Fernandez, J.E., Moreno, F., Giron, I.F., Blazquez, O.M., 1997. Stomatal control of water use in olive tree leaves. Plant and Soil 190 (2), 179–192. https://doi.org/10.1023/a:1004293026973.

Garcia-Ruiz, J.M., Lopez-Moreno, J.I., Vicente-Serrano, S.M., Lasanta-Martinez, T., Begueria, S., 2011. Mediterranean water resources in a global change scenario. Earth Sci. Rev. 105 (3–4), 121–139. https://doi.org/10.1016/j.earscirev.2011.01.006.

Garratt, J.R., 1999. The Atmospheric Boundary Layer. Cambridge University Press, Cambridge, England.

Gennaretti, F., Ripa, M.N., Gobattoni, F., Boccia, L., Pelerosso, R., 2011. A methodology proposal for land cover change analysis using historical aerial photos. J. Geogr. Regional Plann. 4, 542–556.

Gerten, D., Schaphoff, S., Haberlandt, U., Lucht, W., Sitch, S., 2004. Terrestrial vegetation and water balance – hydrological evaluation of a dynamic global vegetation model. J. Hydrol. 286 (1–4), 249–270. https://doi.org/10.1016/j.jhydrol.2003.09.029.

Gim, H.J., et al., 2020. Improved mapping and change detection of the start of the crop growing season in the US Corn Belt from long-term AVHRR NDVI. Agric. For. Meteorol. 294 https://doi.org/10.1016/j.agrformet.2020.108143.

Giorgi, F., 2006. Climate change hot-spots. Geophys. Res. Lett. 33 (8) https://doi.org/10.1029/2006gl025734.

Giorgi, F., Bi, X., Pal, J.S., 2004. Mean, interannual variability and trends in a regional climate change experiment over Europe. I. Present-day climate (1961–1990). Clim. Dyn. 22, 733–756. https://doi.org/10.1007/s00382-004-0409-x.

Giorgi, F., Lionello, P., 2008. Climate change projections for the Mediterranean region. Global Planet. Change 63 (2–3), 90–104. https://doi.org/10.1016/j.gloplacha.2007.09.005.

Giza, A., Terefenko, P., Komorowski, T., Czaplinski, P., 2021. Determining long-term land cover dynamics in the south baltic coastal zone from historical aerial photographs. Remote Sens. (Basel) 13 (6). https://doi.org/10.3390/rs13061068.

Gorguner, M., Kavvas, M.L., 2020. Modeling impacts of future climate change on reservoir storages and irrigation water demands in a Mediterranean basin. Sci. Total Environ. 748 https://doi.org/10.1016/j.scitotenv.2020.141246.

Granier, A., 1987. Evaluation of transpiration in a Douglas-fir stand by means of sap flow measurements. Tree Physiol. 3 (4), 309–320. https://doi.org/10.1093/treephys/3.4.309.

Grossiord, C., et al., 2017. Precipitation, not air temperature, drives functional responses of trees in semi-arid ecosystems. J. Ecol. 105 (1), 163–175. https://doi.org/10.1111/1365-2745.12662.

Hanson, J.D., Skiles, J.W., Parton, W.J., 1988. A multi-species model for rangeland plant communities. Ecol. Model. 44 (1–2), 89–123. https://doi.org/10.1016/0304-3800(88)90084-1.

Helsel, D.R., Hirsch, R.M., Ryberg, K.R., Archfield, S.A., and Gilroy, E.J., 2020, Statistical methods in water resources: U.S. Geological Survey Techniques and Methods, book 4, chap. A3, 458 p. https://doi.org/10.3133/tm4a3.

Hersbach, H., et al., 2020. The ERA5 global reanalysis. Q. J. R. Meteorol. Soc. 146 (730), 1999–2049. https://doi.org/10.1002/qj.3803.

Hersbach, H., Bell, B., Berrisford, P., Biavati, G., Horányi, A., Muñoz Sabater, J., Thépaut, J.N., 2018. ERA5 hourly data on single levels from 1959 to present: 5–6.

Heubes, J., et al., 2011. Modelling biome shifts and tree cover change for 2050 in West Africa. J. Biogeogr. 38 (12), 2248–2258. https://doi.org/10.1111/j.1365-2699.2011.02560.x.

Hickler, T., et al., 2012. Projecting the future distribution of European potential natural vegetation zones with a generalized, tree species-based dynamic vegetation model. Glob. Ecol. Biogeogr. 21 (1), 50–63. https://doi.org/10.1111/j.1466-8238.2010.00613.x.

Hill, T.C., Quaife, T., Williams, M., 2011. A data assimilation method for using low-resolution Earth observation data in heterogeneous ecosystems. J. Geophys. Res.-Atmos. 116 https://doi.org/10.1029/2010jd015268.
Hirsch, R.M., Slack, J.R., Smith, R.A., 1982. Techniques of trend analysis for monthly water quality data. Water Resour. Res. 18 (1), 107–121. https://doi.org/10.1029/WR018i001p00107.
Hu, Y., Maskey, S., Uhlenbrook, S., 2012. Trends in temperature and rainfall extremes in the Yellow River source region, China. Clim. Change 110, 403–429. https://doi.org/10.1007/s10584-011-0056-2.
Jarvis, P.G., 1976. The interpretation of the variations in leaf water potential and stomatal conductance found in canopies in the field. Philos. Trans. R. Soc. B 273 (927), 593–610. https://doi.org/10.1098/rstb.1976.0035.
Kendall, M.G., 1938. A new measure of rank correlation. Biometrika 30 (1–2), 81–93. https://doi.org/10.2307/2332226.
Kurc, S.A., Small, E.E., 2004. Dynamics of evapotranspiration in semiarid grassland and shrubland ecosystems during the summer monsoon season, central New Mexico. Water Resour. Res. 40 (9) https://doi.org/10.1029/2004wr003068.
Larcher, W., 1995. Physiological Plant Ecology. Springer, third ed.: 506.
Levis, S., Bonan B., M., V., Oleson, K., 2004. The community land model's dynamic global vegetation model (CLM-DGVM): technical description and user's guide. doi: https://doi.org/10.5065/D6P26W36.
Li, X.J., et al., 2017. Assimilating leaf area index of three typical types of subtropical forest in China from MODIS time series data based on the integrated ensemble Kalman filter and PROSAIL model. ISPRS J. Photogramm. Remote Sens. 126, 68–78. https://doi.org/10.1016/j.isprsjprs.2017.02.002.
Li, S., Kang, S., Zhang, L., Li, F., Hao, X., Ortega-Farias, S., Guo, W., Ji, S., Wang, J., Jiang, X., 2013. Quantifying the combined effects of climatic, crop and soil factors on surface resistance in a maize field. J. Hydrol. 489, 124–134. https://doi.org/10.1016/j.jhydrol.2013.03.002.
Lionello, P., Scarascia, L., 2018. The relation between climate change in the Mediterranean region and global warming. Reg. Environ. Chang. 18 (5), 1481–1493. https://doi.org/10.1007/s10113-018-1290-1.
Lo Gullo, M., Salleo, S., 1988. Different strategies of drought resistance in three Mediterranean sclerophyllous trees growing in the same environmental conditions. New Phytol. 108 (3), 267–276. https://doi.org/10.1111/j.1469-8137.1988.tb04162.x.
Lumaret, R., Ouazzani, N., 2001. Ancient wild olives in Mediterranean forests. Nature 413, 700. https://doi.org/10.1038/35099680.
Marras, P.A., et al., 2021. Future precipitation in a Mediterranean island and streamflow changes for a small basin using EURO-CORDEX regional climate simulations and the SWAT model. J. Hydrol. 603 https://doi.org/10.1016/j.jhydrol.2021.127025.
Martínez-Fernández, J., Sánchez, N., Herrero-Jiménez, C.M., 2013. Recent trends in rivers with near-natural flow regime: the case of the river headwaters in Spain. Prog. Phys. Geogr.-Earth Environ. 37 (5), 685–700. https://doi.org/10.1177/0309133313496834.
May, W., 2008. Potential future changes in the characteristics of daily precipitation in Europe simulated by the simulated by the HIRHAM regional climate model. Clim Dyn 30, 581–603. https://doi.org/10.1007/s00382-007-0309-y.
Mboga, N., et al., 2020. Fully convolutional networks for land cover classification from historical panchromatic aerial photographs. ISPRS J. Photogramm. Remote Sens. 167, 385–395. https://doi.org/10.1016/j.isprsjprs.2020.07.005.
Mohsin, T., Gough, W.A., 2010. Trend analysis of long-term temperature time series in the Greater Toronto Area (GTA). Theor. Appl. Climatol. 101, 311–327. https://doi.org/10.1007/s00704-009-0214-x.
Montaldo, N., et al., 2021. Rock water as a key resource for patchy ecosystems on shallow soils: digging deep tree clumps subsidize surrounding surficial grass. Earths Future 9 (2). https://doi.org/10.1029/2020ef001870.
Montaldo, N., Albertson, J.D., 2001. On the use of the force-restore SVAT model formulation for stratified soils. J. Hydrometeorol. 2 (6), 571–578. https://doi.org/10.1175/1525-7541(2001)002<0571:OTUOTF>2.0.CO;2.
Montaldo, N., Oren, R., 2018. Changing seasonal rainfall distribution with climate directs contrasting impacts at evapotranspiration and water yield in the western Mediterranean Region. Earths Future 6 (6), 841–856. https://doi.org/10.1029/2018ef000843.
Montaldo, N., Oren, R., 2022. Rhizosphere water content drives hydraulic redistribution: Implications of pore-scale heterogeneity to modeling diurnal transpiration in water-limited ecosystems. Agric. For. Meteorol. 312 https://doi.org/10.1016/j.agrformet.2021.108720.
Montaldo, N., Sarigu, A., 2017. Potential links between the North Atlantic Oscillation and decreasing precipitation and runoff on a Mediterranean area. J. Hydrol. 553, 419–437. https://doi.org/10.1016/j.jhydrol.2017.08.018.
Montaldo, N., Rondena, R., Albertson, J.D., Mancini, M., 2005. Parsimonious modeling of vegetation dynamics for ecohydrologic studies of water-limited ecosystems. Water Resour. Res. 41 (10) https://doi.org/10.1029/2005wr004094.
Montaldo, N., Albertson, J.D., Mancini, M., 2008. Vegetation dynamics and soil water balance in a water-limited Mediterranean ecosystem on Sardinia, Italy. Hydrol. Earth Syst. Sci. 12 (6), 1257–1271. https://doi.org/10.5194/hess-12-1257-2008.
Montaldo, N., Corona, R., Albertson, J.D., 2013. On the separate effects of soil and land cover on Mediterranean ecohydrology: two contrasting case studies in Sardinia, Italy. Water Resour. Res. 49 (2), 1123–1136. https://doi.org/10.1029/2012wr012171.
Montaldo, N., Curreli, M., Corona, R., Oren, R., 2020. Fixed and variable components of evapotranspiration in a Mediterranean wild-olive - grass landscape mosaic. Agric. For. Meteorol. 280 https://doi.org/10.1016/j.agrformet.2019.107769.
Montaldo, N., Gaspa, A., Corona, R., 2023. Assimilation of NDVI data in a land surface – vegetation model for leaf area index predictions in a tree-grass ecosystem. Int. J. Digital Earth 16 (1), 3810–3837. https://doi.org/10.1080/17538947.2023.2259226.
Moore, G.W., Heilman, J.L., 2011. Proposed principles governing how vegetation changes affect transpiration. Ecohydrology 4 (3), 351–358. https://doi.org/10.1002/eco.232.
Nadezhdina, N., et al., 2015. Water uptake and hydraulic redistribution under a seasonal climate: long-term study in a rainfed olive orchard. Ecohydrology 8 (3), 387–397. https://doi.org/10.1002/eco.1545.
Ngadze, F., Mpakairi, K.S., Kavhu, B., Ndaimani, H., Maremba, M.S., 2020. Exploring the utility of Sentinel-2 MSI and Landsat 8 OLI in burned area mapping for a heterogenous savannah landscape. PLoS One 15 (5). https://doi.org/10.1371/journal.pone.0232962.
Nie, F.N., Nie, Y.P., Chen, H.S., Ding, Y.L., Yang, J., Wang, K.L., et al., 2017. Comparison of rooting strategies to explore rock fractures for shallow soil-adapted tree species with contrasting aboveground growth rates: a greenhouse microcosm experiment. Front. Plant Sci. 8, 1651–1661. https://doi.org/10.3389/fpls.2017.01651.
Noilhan, J., Planton, S., 1989. A simple parameterization of land surface processes for meteorological models. Montly. Weather Rev. 117, 536–549. https://doi.org/10.1175/1520-0493(1989)117<0536:ASPOLS>2.0.CO;2.
Nouvellon, Y., et al., 2000. Modelling of daily fluxes of water and carbon from shortgrass steppes. Agric. For. Meteorol. 100 (2–3), 137–153. https://doi.org/10.1016/s0168-1923(99)00140-9.
Olsoy, P.J., Mitchell, J., Glenn, N.F., Flores, A.N., 2017. Assessing a multi-platform data fusion technique in capturing spatiotemporal dynamics of heterogeneous dryland ecosystems in topographically complex Terrain. Remote Sens. (Basel) 9 (10). https://doi.org/10.3390/rs9100981.
Ozturk, T., Ceber, Z.P., Turkes, M., Kurnaz, M.L., 2015. Projections of climate change in the Mediterranean Basin by using downscaled global climate model outputs. Int. J. Climatol. 35 (14), 4276–4292. https://doi.org/10.1002/joc.4285.
Pang, X.X., et al., 2021. Long term variation of evapotranspiration and water balance based on upscaling eddy covariance observations over the temperate semi-arid grassland of China. Agric. For. Meteorol. 308 https://doi.org/10.1016/j.agrformet.2021.108566.
Parlange, M.B., Albertson, J.D., Eichinger, W.E., Cahill, A.T., Jackson, T., 1999. Evaporation: use of fast response turbulence sensors, Raman lidar and passive microwave remote sensing. Vadose Zone Hydrol. doi:10.1093/oso/9780195109900.003.0014.
Philip, J.R., 1957. The theory of infiltration: 1. The infiltration equation and its solution. SoilScience 83(5).
Piras, M., Mascaro, G., Deidda, R., Vivoni, E.R., 2014. Quantification of hydrologic impacts of climate change in a Mediterranean basin in Sardinia, Italy, through high-resolution simulations. Hydrol. Earth Syst. Sci. 18 (12), 5201–5217. https://doi.org/10.5194/hess-18-5201-2014.
Pulighe, G., Lupia, F., Chen, H., Yin, H., 2021. Modeling climate change impacts on water balance of a Mediterranean watershed using SWAT+. Hydrology 8 (4), 157. https://doi.org/10.3390/hydrology8040157.
Ramos, M., 2001. Rainfall distribution patterns and their change over time in a Mediterranean area. Theor. Appl. Climatol. 69, 163–170. https://doi.org/10.1007/s007040170022.
Ramos, A.F., Santos, F.L., 2009. Water use, transpiration, and crop coefficients for olives (cv. Cordovil), grown in orchards in Southern Portugal. Biosyst. Eng. 102(3), 321–333. DOI:10.1016/j.biosystemseng.2008.12.006.
Reick, C.H., Raddatz, T., Brovkin, V., Gayler, V., 2013. Representation of natural and anthropogenic land cover change in MPI-ESM. J. Adv. Model. Earth Syst. 5 (3), 459–482. https://doi.org/10.1002/jame.20022.
Rempe, D.M., Dietrich, W.E., 2018. Direct observations of rock moisture, a hidden component of the hydrologic cycle. Proc. Natl. Acad. Sci. U.S.A. 115(11), 2664–2669. DOI:10.1073/pnas.1800141115.
Salis, M., Ager, A.A., Alcasena, F.J., Arca, B., Finney, M.A., Pellizzaro, G., Spano, D., 2015. Analyzing seasonal patterns of wildfire exposure factors in Sardinia, Italy. Environ. Monit. Assess. 187 https://doi.org/10.1007/s10661-014-4175-x.
Sankaran, M., et al., 2005. Determinants of woody cover in African savannas. Nature 438 (7069), 846–849. https://doi.org/10.1038/nature04070.
Scholes, R.J., Archer, S.R., 1997. Tree-grass interactions in savannas. Annu. Rev. Ecol. Syst. 28, 517–544. https://doi.org/10.1146/annurev.ecolsys.28.1.517.
Schwinning, S., 2010. The ecohydrology of roots in rocks. Ecohydrology 3 (2), 238–245. https://doi.org/10.1002/eco.134.
Sen, P.K., 1968. Estimates of the regression coefficient based on Kendall's tau. J. Am. Stat. Assoc. 63, 1379–1389. https://doi.org/10.2307/2285891.
Sirigu, S., Montaldo, N., 2022. Climate change impacts on the water resources and vegetation dynamics of a forested Sardinian basin through a distributed ecohydrological model. Water 14 (19). https://doi.org/10.3390/w14193078.
Sitch, S., et al., 2003. Evaluation of ecosystem dynamics, plant geography and terrestrial carbon cycling in the LPJ dynamic global vegetation model. Glob. Chang. Biol. 9 (2), 161–185. https://doi.org/10.1046/j.1365-2486.2003.00569.x.
Sneyers, R., 1990. On the statistical analysis of series of observations. Technical Note – World Meteorological Organization 143:192. ISBN: 19912451385.
Song, X., Zeng, X., Zhu, J., 2013. Evaluating the tree population density and its impacts in CLM-DGVM. Adv. Atmos. Sci. 30 (1), 116–124.
Sperry, J.S., Love, D.M., 2015. What plant hydraulics can tell us about responses to climate-change droughts. New Phytol. 207 (1), 14–27. https://doi.org/10.1111/nph.13354.
Swart, N.C., et al., 2019. CCCma CanESM5 model output prepared for CMIP6 C4MIP. Earth Syst. Grid Feder. https://doi.org/10.22033/ESGF/CMIP6.1301.

Terral, J.F., et al., 2004. A hydraulic conductivity model points to post-Neogene survival of the Mediterranean olive. Ecology 85 (11), 3158–3165. https://doi.org/10.1890/03-3081.

Theil, H., 1950. A Rank-Invariant Method of Linear and Polynomial Regression Analysis. In: Raj, B., Koerts, J. (Eds.). Henri Theil's Contributions to Economics and Econometrics. Advanced Studies in Theoretical and Applied Econometrics, vol. 23. Springer, Dordrecht. https://doi.org/10.1007/978-94-011-2546-8_20.

Verkaik, I., et al., 2013. Fire as a disturbance in mediterranean climate streams. Hydrobiologia 719 (1), 353–382. https://doi.org/10.1007/s10750-013-1463-3.

Villegas, J.C., Espeleta, J.E., Morrison, C.T., Breshears, D.D., Huxman, T.E., 2014. Factoring in canopy cover heterogeneity on evapotranspiration partitioning: beyond big-leaf surface homogeneity assumptions. J. Soil Water Conserv. 69 (3), 78A–83A. https://doi.org/10.2489/jswc.69.3.78A.

Williams, A.P., et al., 2013. Temperature as a potent driver of regional forest drought stress and tree mortality. Nat. Clim. Chang. 3 (3), 292–297. https://doi.org/10.1038/nclimate1693.

Yang, X., Crews, K.A., Yan, B., 2016. Analysis of the pattern of potential woody cover in Texas savanna. Int. J. Appl. Earth Obs. Geoinf. 52, 527–531. https://doi.org/10.1016/j.jag.2016.07.021.

Yang, C., Lei, H.M., 2022. Climate and management impacts on crop growth and evapotranspiration in the North China Plain based on long-term eddy covariance observation. Agric. For. Meteorol. 325 https://doi.org/10.1016/j.agrformet.2022.109147.

Yaseef, N.R., Yakir, D., Rotenberg, E., Schiller, G., Cohen, S., 2010. Ecohydrology of a semi-arid forest: partitioning among water balance components and its implications for predicted precipitation changes. Ecohydrology 3 (2), 143–154. https://doi.org/10.1002/eco.65.

Yu, K.L., D'Odorico, P., 2014. Climate, vegetation, and soil controls on hydraulic redistribution in shallow tree roots. Adv. Water Resour. 66, 70–80. https://doi.org/10.1016/j.advwatres.2014.02.003.

Yuan, W.P., et al., 2019. Increased atmospheric vapor pressure deficit reduces global vegetation growth. Sci. Adv. 5 (8) https://doi.org/10.1126/sciadv.aax1396.

Zheng, H., et al., 2023. Divergent environmental responses of long-term variations in evapotranspiration over four grassland ecosystems in China based on eddy-covariance measurements. J. Hydrol. 625 https://doi.org/10.1016/j.jhydrol.2023.130030.

Zhu, K., Woodall, C.W., Monteiro, J.V.D., Clark, J.S., 2015. Prevalence and strength of density-dependent tree recruitment. Ecology 96 (9), 2319–2327. https://doi.org/10.1890/14-1780.1.